Hindawi
Advances in Materials Science and Engineering
Volume 2024, Article ID 9840238, 1 page
https://doi.org/10.1155/2024/9840238

Retraction

Retracted: Genetic Algorithm Integrated Fuzzy AHP-VIKOR Approach for the Investigation of W-Cut Insert Heat Exchanger for Cooling of Dielectric Fluid Used in Ultra-High Voltage Transformer

Advances in Materials Science and Engineering

Received 8 January 2024; Accepted 8 January 2024; Published 9 January 2024

This article has been retracted by Hindawi following an investigation undertaken by the publisher [1]. This investigation has uncovered evidence of one or more of the following indicators of systematic manipulation of the publication process:

(1) Discrepancies in scope
(2) Discrepancies in the description of the research reported
(3) Discrepancies between the availability of data and the research described
(4) Inappropriate citations
(5) Incoherent, meaningless and/or irrelevant content included in the article
(6) Manipulated or compromised peer review

The presence of these indicators undermines our confidence in the integrity of the article's content and we cannot, therefore, vouch for its reliability. Please note that this notice is intended solely to alert readers that the content of this article is unreliable. We have not investigated whether authors were aware of or involved in the systematic manipulation of the publication process.

Wiley and Hindawi regrets that the usual quality checks did not identify these issues before publication and have since put additional measures in place to safeguard research integrity.

We wish to credit our own Research Integrity and Research Publishing teams and anonymous and named external researchers and research integrity experts for contributing to this investigation.

The corresponding author, as the representative of all authors, has been given the opportunity to register their agreement or disagreement to this retraction. We have kept a record of any response received.

References

[1] N. V. Gowri, J. S. Isaac, T. Muralikrishna et al., "Genetic Algorithm Integrated Fuzzy AHP-VIKOR Approach for the Investigation of W-Cut Insert Heat Exchanger for Cooling of Dielectric Fluid Used in Ultra-High Voltage Transformer," *Advances in Materials Science and Engineering*, vol. 2022, Article ID 2819688, 24 pages, 2022.

Hindawi
Advances in Materials Science and Engineering
Volume 2022, Article ID 2819688, 24 pages
https://doi.org/10.1155/2022/2819688

Research Article

Genetic Algorithm Integrated Fuzzy AHP-VIKOR Approach for the Investigation of W-Cut Insert Heat Exchanger for Cooling of Dielectric Fluid Used in Ultra-High Voltage Transformer

N. Vasantha Gowri,[1] J. Samson Isaac,[2] T. Muralikrishna,[1] G. Suresh Babu,[1] Melvin Victor Depoures ,[3] S. Sekar,[4] P. Sasirekha,[5] M. Ramesh ,[6] and S. Prabhakar [7]

[1]*Department of Electrical and Electronics Engineering, Chaitanya Bharathi Institute of Technology (A), Gandipet 500075, Telangana, India*
[2]*Department of Biomedical Engineering, Surgical and Critical Care Equipments Laboratory, Karunya Institute of Technology and Sciences, Coimbatore 641114, Tamil Nadu, India*
[3]*Department of Thermal Engineering, Saveetha School of Engineering, Saveetha Institute of Medical and Technical Sciences, Chennai 602105, Tamil Nadu, India*
[4]*Department of Mechanical Engineering, Rajalakshmi Engineering College, Thandalam, Chennai 602105, Tamil Nadu, India*
[5]*Department of Electrical and Electronics Engineering, M.Kumarasamy College of Engineering, Karur 639113, Tamil Nadu, India*
[6]*Department of Electrical and Electronic Engineering, Vaageswari College of Engineering, Karimnagar 505527, Telangana, India*
[7]*Department of Mechanical Engineering, Automotive Engineering Stream, Wollo University-KIOT, 208, Kombolcha, Ethiopia*

Correspondence should be addressed to S. Prabhakar; prabhakar@kiot.edu.et

Received 9 May 2022; Revised 27 June 2022; Accepted 4 July 2022; Published 31 July 2022

Academic Editor: Kumarasamy Sathiyasekar

This study proposes a novel W-cut twisted tape to evaluate and enhance the effectiveness of novel grooved tube heat exchanger. The experimental investigations are carried out with W-cut inserts, which possess two main control factors, namely, twist tape ratio ($y = 3.5$ to 6.5) and width tape ratio (WR = 0.43 to 0.6). The investigation results prove that in all cases the energy transmission and friction factor of W-cut insert along with the first law and second law efficiency are considerably higher than the conventional tube arrangement. The empirical model equations for friction factor, performance enhancement ratio, Nusselt number, and rational efficiency are developed, and they show good affinity with experimental data. Since the abovementioned factors have conflicting terms, it is essential to select the proper operating configuration of the heat exchanger in order to increase the thermal energy transfer rate with reduced consumption of pumping energy. The multi-objective genetic algorithm (GA) tool is used to identify the optimum operating conditions. Further, the hybrid multi-criteria decision-making model, FAHP-VIKOR, is applied to select the perfect model from the set of non-dominated solution. The ranking of alternatives is as follows: A4 > A11 > A2 > A9 > A21 > A17 > A1 > A24 > A11 > A23 > A7 > A18 > A13 > A10 > A20 > A5 > A19 > A14 > A16 > A22 > A25 > A6 > A15 > A3 > A8. The optimized configuration of W-cut insert is compared with the former inserts, and the optimal configuration exhibits supreme performance than other inserts.

1. Introduction

The global thirst for energy is constantly increasing. The increased demand for the cost of energy and materials has led to the production of high-performance compact heat exchanger systems. Heat transfer augmentation techniques are often used in several thermal system applications such as air conditioning and refrigeration systems, heat recovery process, and chemical reactors to increase the overall performance. Augmentation methods such as eddy flow devices

(especially twisted tapes) are extensively used in industrial heat exchangers for enhancing convective heat transfer. The presence of typical twisted tape in the tube leads to increased pumping power, which results in thermal performance below unity, so that proper design of twisted tape is required to increase the heat transfer of the equipment with reduced pressure drop [1]. Many research studies have been carried out in past decades to bring down the friction loss by modifying peripheral of twisted tape with different geometry, which includes double V-ribbed twisted tapes [2], horizontal wing-cut TT [3], perforated V-cut and U-cut TT [4], tapered twisted tape [5], TT consisting of wire nails [6], loose-fit perforated twisted tapes [7], twisted tape with alternate axis [8], ribbed twisted tape inserts [9], finned twisted tape [10], cross hollow TT [11], peripherally cut dual TT [12], helix TT with V-cut [13], square and V-cut twisted tape [14], centre-cleared twisted tape [15], dual TT [16], rectangular-cut TT [17], circular tube with lanced ring insert [18], and perforated helical TT [19]. The double V-cut perforated TT with width ratio and twist ratio of 0.27 and 2 enhances the heat transfer by 3.5 times while operating at the flow Reynolds number ranging from 2000 to 25000 [20]. These modified geometry twisted tapes are generally designed to induce enhanced swirl flow near the wall region, which affects the increase in fluid velocity and reduction in boundary layer thickness. This results in augmented heat transfer when compared to typical twisted tape [21]. In general, the performance enhancement ratios of these tapes are higher than the former typical twisted tapes. For instance, the mean performance ratio of the abovementioned tapes is about 2–4 times higher than the typical one. All these aforementioned researches were carried out in plain tube. Wijayanta et al. [22] utilized short-length twisted tape in concentrated tube heat exchangers that improve heater transfer and friction factor by 0.51 and 2.84 times as compared with the conventional heat exchangers for the Reynolds number ranging from 4500 to 18500. Wijayanta et al. [23] compared the thermo-hydraulic performance of classical and square-cut twisted tapes and resulted that the maximum performance of the heat exchangers is ranging from 74.7 to 80.7%. Then, the researchers modified the tabulators into V shapes and enhanced the performance by 97% [24]. Further modifications are carried out in the turbulators by attaching trapezoidal tape winglet that improves the heat transfer and friction factor by 1.91 and 5.2 times, respectively [25]. Yaningsih et al. incorporated perforated holes in the twisted tapes and improved the heater transfer and friction factor performance in the concentric tube heat exchanger by 32% and 47%, respectively [26].

In the recent past, the combined passive method has been extensively used to increase the heat transfer rate. The investigations are carried out with geometrically modified twisted tapes, which are fitted in altered test sections. Most of the researchers revealed that the overall performance of the combined insert performs best compared with the individual ones. Bharadwaj et al. [27] initiated the study on thermal and flow characteristics of the grooved tube fitted with twisted tapes. The grooved tube with twisted tape showed better performance than the simple grooved tube. Kumbhar and Sane [28] made an investigation on heat transfer and pressure drop of the dimpled tube with regularly spaced twisted tape insert. The result showed that full-length twisted tape gave a better performance with dimpled tube. Hong et al. [29] made an experimental study on thermal and friction characteristics of spirally grooved tube fitted with twin overlapped twisted tapes. The function of overlapped tapes in spiral grooved tube was not effective when compared to the simple grooved tube. Verma et al. [30] utilized modified helical coil twisted tapes and improved the heat transfer and friction factor by 3.14 times and 19.9 times as compared with the conventional system. Promvonge et al. [31] studied the effect of twisted ratio on performance characteristics in a helical-ribbed tube with twin TTs. Hong et al. [32] numerically examined the effect of thermal and flow performance of the geometrically modified twin TT's built-in converging-diverging tube. As mentioned above, the combined twisted tape and grooved tube lead to higher heat transfer rate and friction factor than plain tube. Increased Nusselt number results in energy saving, whereas a rise in friction factor upsurges the pumping cost. Hence, the optimization of grooved tube heat exchanger is essential for obtaining high performance with energy saving and pumping cost reduction [33, 34]. Blade vortex generator inserts, multiple helical tape inserts, and diverging perforated cones are special types of inserts that are used as turbulators to reduce the flow blockage in downstream conditions and improve the Reynolds number [35]. Wijayanta et al. [36] proposed that delta wing tape turbulators raise the heat transfer performance by 177% and their design configurations are optimized using the ANN method [37]. The maximum enhancement using T-wing tape tabulator is 1.15 [38]. The double-side winglet integrated twisted tapes raise the Nusselt number by 269% and improve the performance by 10.1 times as compared with plain tube [39, 40]. Veerabhadrappa Bidari et al. [41] modified the turbulators for heat exchangers by punched delta winglet vortex shapes and improved thermo-hydraulic performance by 1.22 times as compared with other systems.

The optimization study to improve the design parameters of concentric heat exchangers has been evoked recently. Han et al. [42] did a multi-objective shape optimization study on corrugated tube double pipe heat exchangers using RSM methods. The maximum performance ratio obtained for the r optimum design parameter is 1.12. Swamee et al. [43] analyzed the optimization of heat exchanger with single degree of difficulty. The solution gives an optimal design for the parameters, which include inner diameter and outer diameter of the pipe, and utility flow rate. Iqbal et al. [44] made an optimization study to determine the optimum shape of longitudinal fins on the outer pipe of the heat exchanger for maximizing the Nusselt number. The result showed that the optimum fin profile offers a Nusselt number, which was about 312% higher than the conventional design.

Iqbal et al. [45] designed an optimal configuration of a finned annulus with parabolic fins to enhance the heat transfer. As a result, the optimal configuration of parabolic fins is not compared with triangular and trapezoidal fin in all

situations and criteria. Despite various researches being carried out on combined passive techniques, very few researchers focused on the optimization of the insert configurations used in heat exchangers. This shortage creates research gap for upcoming researchers to narrow their investigation. The main objective of this study was to perform optimization on design and operating configurations of WCTT fitted in grooved tube heat exchanger using the genetic algorithm and multi-criteria decision-making model.

The genetic algorithm is the searching tool that is available for solving problems when the functional characters are unknown. Some of the researchers used GA to optimize the objective parameters of heat exchangers in order to attain the overall best performance [46, 47]. After a thorough analysis on the performance of the heat exchanger with the effect of WCTT geometrical parameters, the new experimental correlations were developed to predict the Nusselt number and friction factor of the tube under the defined range. These correlations were used as the objective function to find the optimal Pareto front solutions. As the given objectives are conflicting terms, GA-based multi-objective optimization is used to attain optimal configurations. Yet, it was difficult to find the best configuration with MOGA, as all the solutions obtained were optimal. Therefore, this study focuses on achieving the best one using a hybrid MCDM model with four performance criteria. The novel FAHP-VIKOR model is used to evaluate alternative configurations and select the best one with conflicting criteria. The application of MCDM in heat transfer area is very meagre [48, 49]. According to the findings, there is research being done on the selection of twisted tape configurations based on thermal and exergy performance using MCDM models. In this work, the FAHP-VIKOR model is used to select the best from the optimum Pareto front solutions of GA. The structure of the present work is given in Figure 1, and their stages are as follows: (i) initially the experimentation is done and the empirical correlations were developed; (ii) followed by multi-objective GA optimization tool to get set of optimum Pareto solution; (iii) finally, assessment method, which includes FAHP-VIKOR model to rank the optimum Pareto front of GA.

2. Experimental Work

2.1. Twisted Tapes and Grooved Tube. The WCTT is made of aluminium sheets with a width of 0.0235 m, a thickness of 0.003 m, and a length of tape of 1500 mm. Initially, plain twisted tapes are made by twisting one end of the tape at the desired twist tape ratio ($y = 3.5$ to 6.4), while the other end is clamped. Then, a W-shaped element is removed from the peripheral of the plain tape with a given width ratio (WR = 0.45, 0.6). In this work, the width ratio is defined as the ratio of the width of the W-cut to the width of the twisted tape. The test section used in this setup is an internally grooved tube, which is composed of internal grooves in the plain copper tube with a specified pitch. These values are fixed based on the boundary layer thickness formulation while maintaining the flow Reynolds number ranging from 3000 to 15000. The cut section of the grooved tube is shown in Figure 2, and the geometry of WCTT is depicted in Table 1 and Figure 3.

2.2. Experimental Apparatus and Test Procedure. Figure 4 represents the schematic diagram of experimental setup of double pipe heat exchanger. The system comprises of calming section, test section (smooth or grooved tube) for transformer mineral oil flow, and outer tube for cold-water flow. The calming section and test sections are made of copper tubes with diameter, length, and thickness of 25 mm, 1500 mm, and 1.5 mm, respectively. The outer tube is made of steel tubes with diameter of 52 mm, thickness of 4 mm, and length of 1500 mm. The outer tube is covered with insulation materials such as foam, asbestos, and glass wool to avoid heat loss to the environment. Some other components of heat exchanger include pump, rotameter, control valves, hot and cold-water tank, fan, and control switches. Besides, U-tube manometer and K-type thermocouples were positioned at inlet and outlet of the test section and outer tube to measure the pressure drop and bulk temperatures of the flow. The temperature of the transformer mineral oil is maintained constantly at 55°C using a temperature sensor and relay control unit, while the cold water is maintained at room temperature. The test procedure follows two sections, namely, transformer mineral oil loop and cold-water loop. In the transformer mineral oil loop, the electric heater with 4 KW is used to heat the water. After reaching the specified temperature, the transformer mineral oil is allowed to flow through calming section followed by the test section and it returns to transformer mineral oil tank. As the transformer mineral oil dissipates a certain temperature to the cold water, loss of temperature is noted. To maintain the set temperature, sensor with temperature control relay is used to maintain the transformer mineral oil tank with fixed temperature. Similarly, the same procedure is followed in cold-water loop section. In this, the cold water at room temperature is allowed to flow through the outer pipe and it takes some temperature from the transformer mineral oil. To maintain cold-water temperature, a cooling section is made in which the added temperature nullifies and returns to the cold-water tank with set temperature. The K-type thermocouples with 0.1°C accuracy are used to measure the surface temperature of the internal tube. They are set up at equal distances from the inlet. An 8 mm steel tube is used to protect the thermocouple from direct contact with the water in the annulus section. This tube is brazed to both the outside and inside tubes of the test sections. Experimentation is conducted to determine the thermal performance of heat exchanger at flow rates of 2–10 LPM for transformer mineral oil and constant 10 LPM for cold water. The temperature and pressure of the fluid at inlet and outlet and the surface temperature are measured under steady-state conditions. The details of experimentation are specified in Table 1. Each experiment is repeated three times to ensure its accuracy and repeatability.

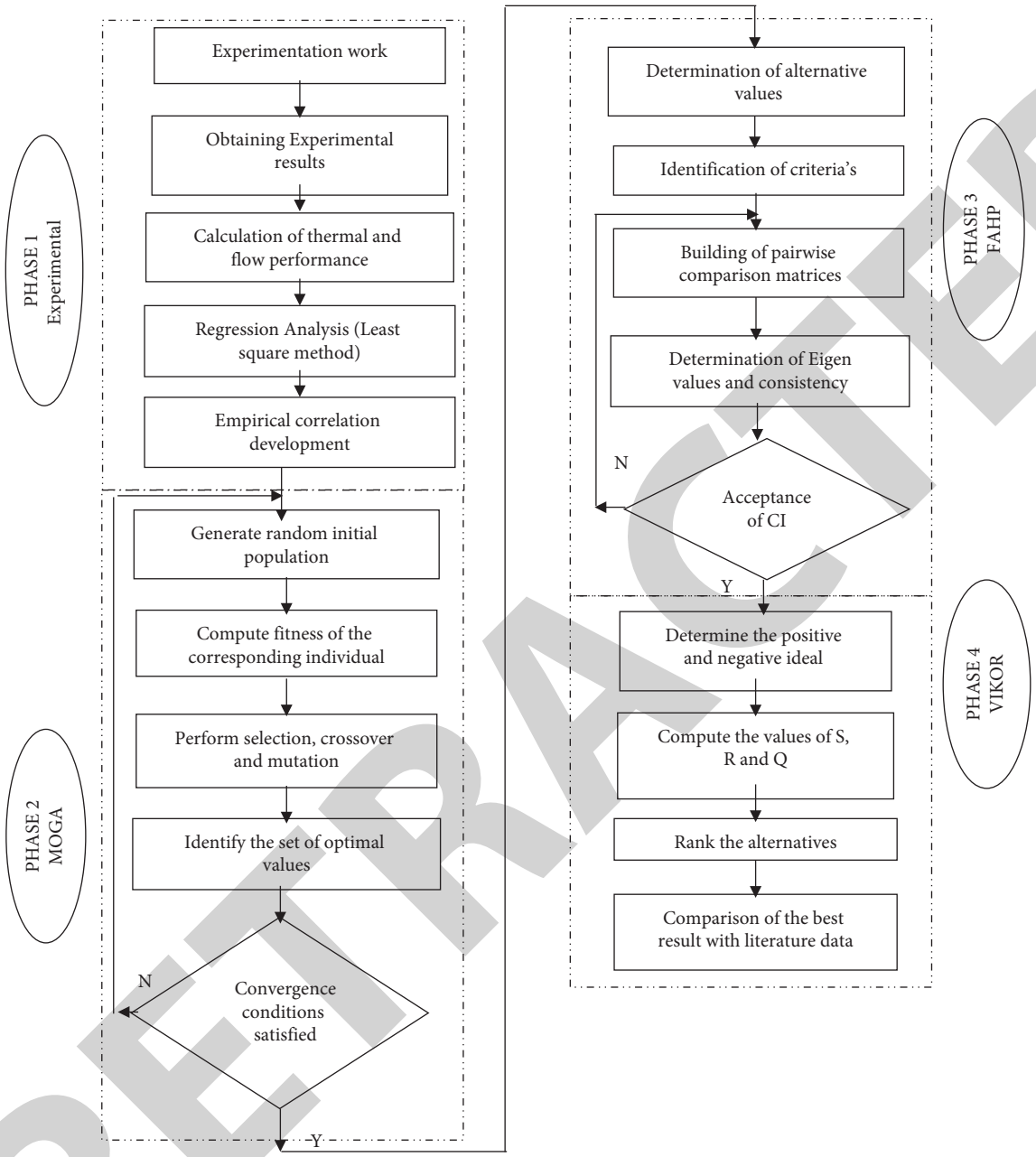

Figure 1: Phases of evaluation procedure.

3. Experimental Calculation

3.1. Data Reduction. The formulas used to obtain the overall performance of the inserts are as follows.

The average of inlet and outlet temperature is taken as bulk temperature, which is expressed as follows:

$$T_C = \frac{T_{ci} + T_{c0}}{2}, \qquad T_h = \frac{T_{hi} + T_{ho}}{2}. \tag{1}$$

The heat transferred to cold water is provided as follows:

$$Q_C = m_c C_p (T_{co} - T_{ci}). \tag{2}$$

Heat rejected from the transformer mineral oil is given as follows:

$$Q_h = m_h c_p (T_{hi} - T_{ho}). \tag{3}$$

Assume that the working fluid has a mean temperature of

$$Q_{avg} = \frac{Q_c + Q_h}{2}. \tag{4}$$

The surface temperature of the tube is given as follows:

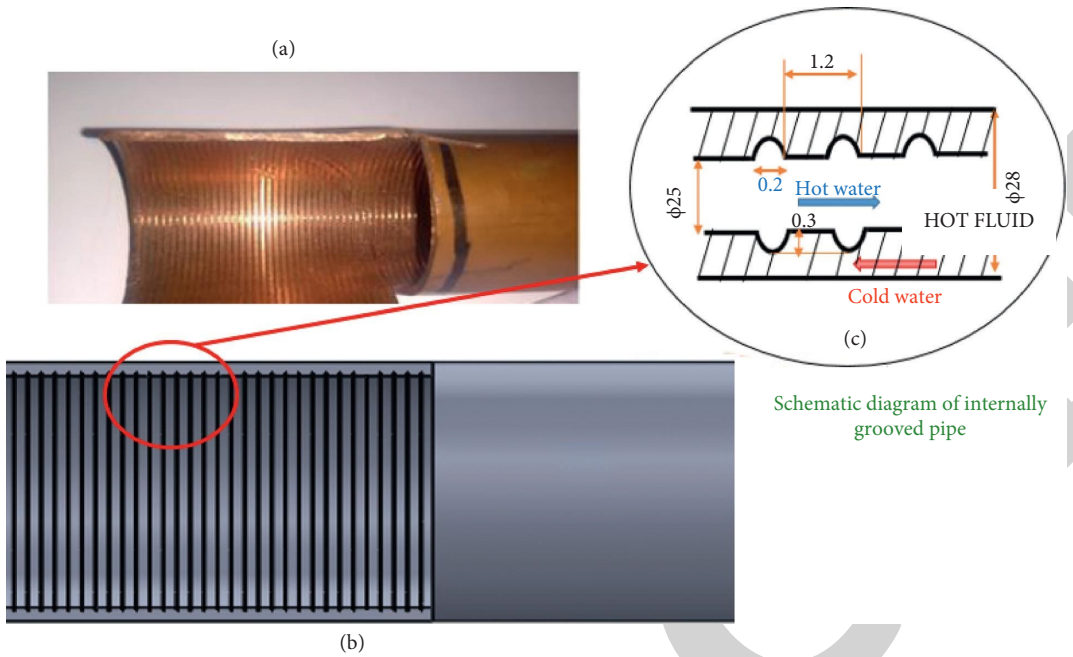

Figure 2: Cut section of internally grooved test section: (a) grooved copper pipe, (b) 3D model of grooved pipe, (c) schematic of groove.

Table 1: Experimental details.

Test tube condition (A)	
Outer diameter of heat exchanger's inner tube	50.5 mm
Inner diameter of heat exchanger's inner tube	25 mm
Reynolds number	3000–15000
Inlet transformer mineral oil temperature	55°C
Length (L)	1500 mm
Groove pitch (P)	1.2 mm
Groove thickness (X)	0.2 mm
Groove height (e)	0.3 mm
Inlet cold-water temperature	31°C
W-cut TT (B)	
Pitch tape length (H)	83, 125, and 150 mm
Tape width (W)	23.5 mm
Depth of the cut	10 mm
Configuration used	W-cut TT
Twist tape ratio (y)	3.5, 5.3 and 6.5
Tape thickness	3 mm
Width ratio (WR)	0.45 and 0.6

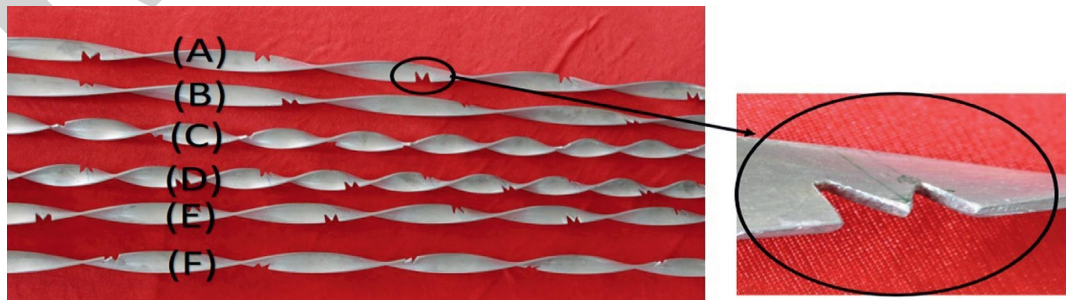

Figure 3: Configuration of W-cut TT: (a) $y = 6.4$, WR = 0.6; (b) $y = 6.4$, WR = 0.45; (c) $y = 5.3$, WR = 0.6; (d) $y = 5.3$, WR = 0.45; (e) y of 5.3, WR = 0.6; (f) y of 5.3, WR = 0.45.

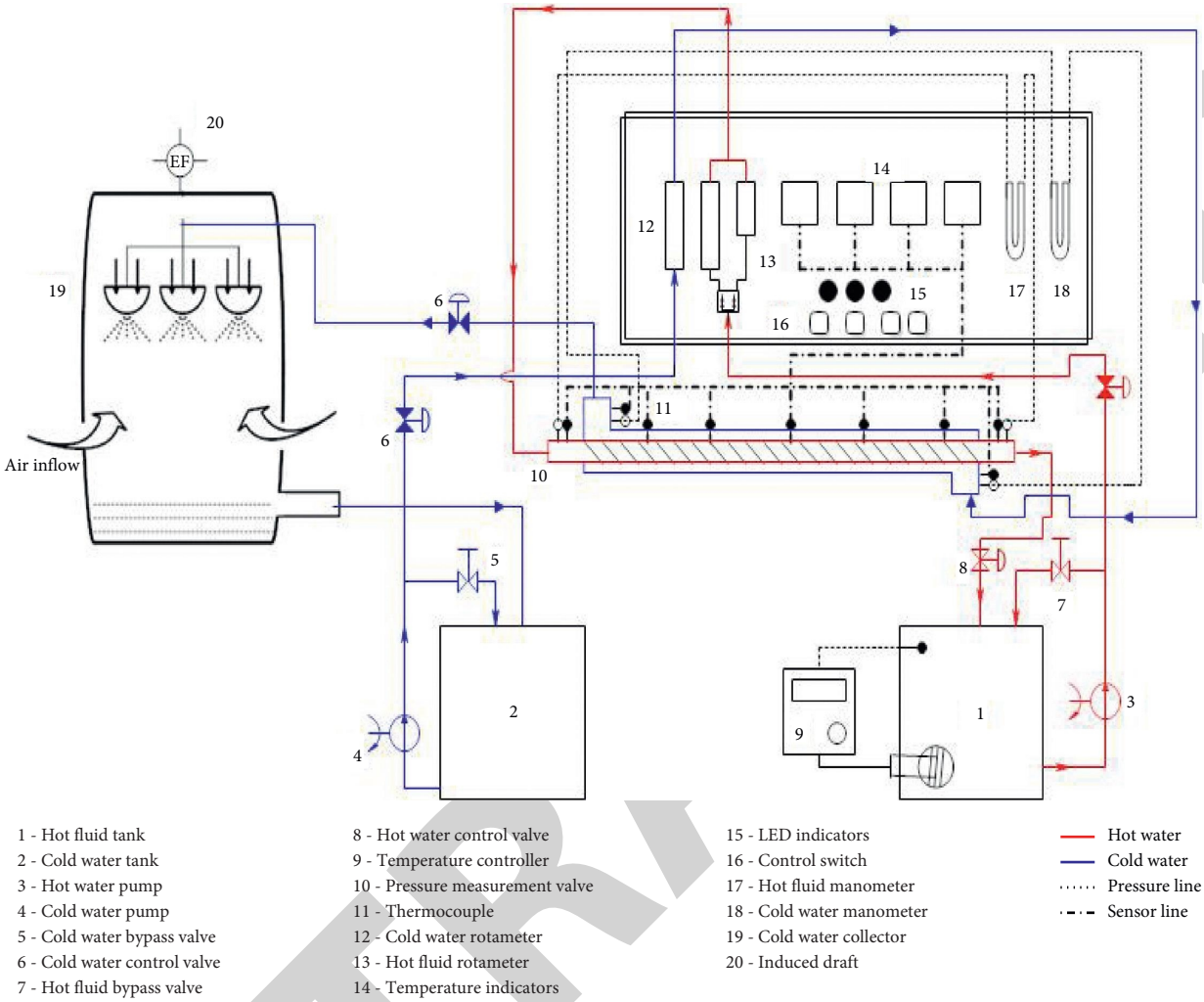

Figure 4: Schematic diagram of experimental rig.

$$T_W = \frac{\sum T_{wi}}{5}. \tag{5}$$

The average Nusselt number and average heat transfer coefficient of inner section can be calculated as follows:

$$h_i = \frac{Q_{avg}}{A(T_h - T_W)}, \qquad Nu_i = \frac{h_i d_h}{k}. \tag{6}$$

Equation (7) is used to evaluate the Reynolds number given as follows:

$$\mathrm{Re} = \frac{U_h d_h}{\nu}. \tag{7}$$

The friction factor due to fluid flow is evaluated as a function of pressure drop given as follows:

$$f = \frac{\Delta p}{(L/d_h)(\rho u^2/2)}. \tag{8}$$

The usage of novel W-cut twisted tape and conventional plain tube is compared based on the calculated value of the term performance enhancement factor given as follows:

$$PER = \frac{Nu/Nu_o}{(f/f_o)^{1/3}}. \tag{9}$$

The above equation (9) is used to calculate PER in Section 5.4.

3.2. Exergy Analysis. Rational efficiency also known as exergy efficiency or second law efficiency analyses the efficiency of the system by considering the second law of thermodynamics. The rational efficiency of the heat exchanger is defined as the ratio of net exergy output of the system to net exergy input. In this study, second law efficiency is availed to enhance and select the dimensions for the heat exchanger. In general, the qualitative energy of exergy balance is given as follows [50]:

$$E_{in} - E_{out} = I. \tag{10}$$

From the equation (10), the net rate of exergy of the heat exchanger is given as follows:

$$E^{in} = \sum_{i=1}^{N.stream.In} m_i E^{in}_{stream,i} + \sum_{i=1}^{N.Q.In} m_i E^{in}_{Q,i} + \sum_{i=1}^{N.W.In} m_i E^{in}_{W,i},$$
$$E^{out} = \sum_{i=1}^{N.stream.Out} m_i E^{out}_{stream,i} + \sum_{i=1}^{N.Q.out} m_i E^{out}_{Q,i} + \sum_{i=1}^{N.W.Out} m_i E^{out}_{W,i}. \quad (11)$$

The exergy balance for the fluids in heat exchanger [51] can be stated as follows:

$$E^{in} = E^{out}_{useful} + E^{out}_{waste} + I. \quad (12)$$

The rate of exergy destruction in terms of generation of entropy is given as follows:

$$I = T_o \dot{S}_{gen}. \quad (13)$$

For the concentric heat exchanger, the entropy generation (13) can be written as follows:

$$\dot{S_{gen}} = m_h C_{ph} \ln\left(\frac{T_{h,out}}{T_{h,in}}\right) + m_c C_{pc} \ln\left(\frac{T_{c,out}}{T_{c,in}}\right) + m_h \frac{\Delta P_h}{\rho_h} \frac{\ln T_{h,out}/T_{h,in}}{T_{h,out} - T_{h,in}} + m_c \frac{\Delta P_c}{\rho_c} \frac{\ln T_{c,out}/T_{c,in}}{T_{c,out} - T_{c,in}}. \quad (14)$$

The "exergy output attained" divided by "used exergy" gives the value of rational exergy efficiency stated in the following equation [52]:

$$\varepsilon = 1 - \frac{I}{E_{used}}. \quad (15)$$

The overall performance of the system based on the second law is represented by the following equation [53]:

$$E_{used} = E_{obtainedoutput} + I. \quad (16)$$

The aforementioned system's goal to increase the thermal exergy of the hot stream is given as follows:

$$E_{obtainedoutput} = E_h^{\Delta T,out} - E_h^{\Delta T,in}. \quad (17)$$

Then, by combining equations (16) and (17), the useful value of exergy is given as follows:

$$E_{used} + I = E_c^{\Delta p,in} + E_h^{\Delta P,in} + E_c^{\Delta T,in} - E_c^{\Delta T,out} + E_h^{\Delta P,out} + E_c^{\Delta P,out}. \quad (18)$$

The system's overall rational exergy efficiency is given as follows:

$$\eta_{II} = \frac{\sum (\dot{E})_{out}}{\sum (\dot{E})_{in}}, \quad (19)$$

$$\eta_{II} = \frac{m_h C_{ph} \ln\left(T_{h,out}/T_{h,in}\right)}{m_c C_{pc} \ln\left(T_{c,out}/T_{c,in}\right) + m_h \Delta P_h/\rho_h \ln T_{h,out}/T_{h,in}/T_{h,out} - T_{h,in} + m_c \Delta P_c/\rho_c \ln T_{c,out}/T_{c,in}/T_{c,out} - T_{c,in}}.$$

The above equation is used to calculate rational exergy efficiency in Section 5.5.

3.3. Uncertainty Analysis. It is possible to calculate the experimental uncertainty of friction factor, Reynolds number, and Nusselt number using the following formulas:

$$\frac{\Delta \mathrm{Re}}{\mathrm{Re}} = \left\{ \left[\frac{\Delta m_h}{m_h}\right]^2 + \left[\frac{\Delta d_i}{d_i}\right]^2 \right\}^{0.5}, \quad (20)$$

$$\frac{\Delta Nu_i}{Nu_i} = \left\{ \left[\frac{\Delta h_i}{h_i}\right]^2 + \left[\frac{\Delta d_i}{d_i}\right]^2 + \left[\frac{\Delta k}{k}\right]^2 \right\}^{0.5}, \quad (21)$$

$$\frac{\Delta f}{f} = \left\{ \left[\frac{\Delta (\Delta P)}{\Delta P}\right]^2 + \left[\frac{\Delta L}{L}\right]^2 + \left[\frac{3\Delta d_i}{d_i}\right]^2 + \left[\frac{2\Delta \mathrm{Re}}{\mathrm{Re}}\right]^2 \right\}^{0.5}. \quad (22)$$

The uncertainties and instrument accuracy of the present work are given in Table 2.

4. Optimization Method

4.1. Multi-Objective Genetic Algorithm (MOGA). Multi-objective optimization (MOO) [54] refers to the solution of problems that deal with more than one objective. In actual engineering problems, most of their objectives are at least in partial conflict with one another. It is difficult to

Table 2: Accuracy of the instruments.

		Accuracy
Instruments	U-tube manometer	±0.0001 m
	Digital thermocouple	±0.1°C
	Rotameter	±0.1 L/min
	Temperature indicators	±0.1%
		Uncertainty (±%)
Simple variable	Pressure head (mm)	2.7
	Temperature (°C)	0.08
		Uncertainty (±%)
Compound variable	Pressure drop (ΔP)	5.55
	Friction factor (f)	4.05
	Nusselt number (Nu)	5.38
	Reynolds number (Re)	2.01
	Heat transfer coefficient (h)	5.38
	Heat transfer (Q)	5.24

detect the maximum or minimum of multi-objectives simultaneously available for single objective optimization. The term MOO generally refers to the set of non-inferior solution points, known as Pareto optimal solutions [38]. The best solution for the multi-objective problem can be selected from the Pareto set rendering to decision-making methods. MOGA is the multi-objective optimization tool for solving problems with more than one design objective, and it has unique supremacy in multi-objective programming. The steps involved in MOGA are as follows:

Step 1: generate random population of chromosomes with a static initial size

Step 2: assess the fitness of the objective function solutions in the population

Step 3: generate new offspring from parent population using selection, crossover, and mutation

Step 4: finally, this process terminates only when the optimal solution is achieved, else it goes to Step 2

Evidently, the offspring population will be comparatively good than the parent population as it undergoes the survival of fittest principle. The solution becomes closer and closer to optimal with gradual evaluation. Finally, when GA is convergent, the set of Pareto front optimized solutions is obtained. In this study, hybrid MCDM (FAHP-VIKOR) is employed to select the finest solution from the set of Pareto front solutions.

4.2. Multi-Criteria Decision-Making (MCDM). Multi-criteria decision-making (MCDM) is a tool, which is used for evaluating the trade-offs between several performance criteria to rank, prioritize, or choose the best from the list of alternatives. The MCDM problem selected in this study is to rank the set of Pareto front solutions (taken as alternatives) obtained from GA. The prioritization of these alternatives is done using the following criteria: thermal enhancement ratio (TER), friction enhancement ratio (FER), performance enhancement ratio (PER), and rational exergetic efficiency (REE). Figure 5 depicts the various criteria used in performance evaluation. In this MCDM model, at the initial stage, the FAHP is used to give weightage for the criteria, followed by the ranking of alternatives with VIKOR.

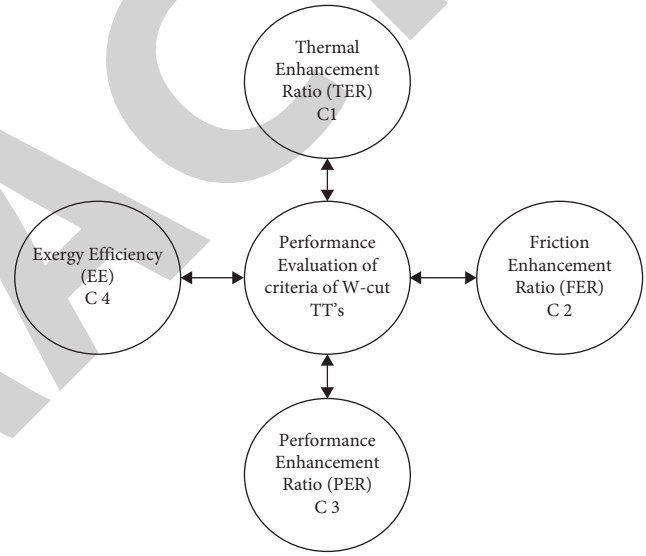

Figure 5: Different criteria for performance evaluation of grooved tube with W-cut twisted insert.

4.2.1. FAHP Method. Satty and decision [55] proposed the AHP method. In AHP, the decision problem is classified into different levels of hierarchy, each level comprising a finite number of elements [56]. A fuzzy set comprises membership function associated in the range of zero and one. Kwong and Bai [46] proposed the concept of fuzzy AHP. FAHP offers triangular and trapezoidal fuzzy number in accordance with the decision-maker need. The authors of past used FAHP tool to assign weightage to their criteria [57, 58]. The hierarchy of decision-making problem is shown in Figure 6. The steps of FAHP method are as follows:

Step 1: complex problem is broken down into simple hierarchy of interconnected criteria.

Step 2: the triangular fuzzy number (TFN) $M = (l, m, u)$ is used to fuzzy the pairwise decision matrix A. The

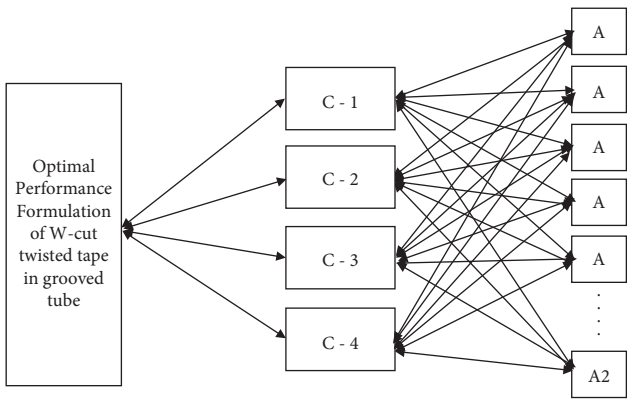

Figure 6: Decision hierarchy for performance prediction of W-cut TT.

membership function of the TFNs used to signify the assessment is M1, M2, M3, M4, M5, M6, M7, M8, and M9 (Table 3). Then, the decision matrix is normalized and the relative weight of each matrix is identified. The expression for eigenvector can be given as follows:

$$A_w = \lambda_{\max} W. \tag{23}$$

Step 3: consistency index (CI) values are identified:

$$CI = \frac{(\lambda_{\max})}{(n-1)}. \tag{24}$$

Step 4:the consistency ratio (CR) is used to define the consistency of the inputs and is given as follows:

$$CR = \frac{(CI)}{(RCI)}. \tag{25}$$

In case the CR value is greater than the acceptable value, inconsistency in judgment occurs and the entire assessment must be reassessed and enhanced. The selection of RCI values based on the number of criteria is given in Table 4.

4.3. VIKOR Method. Opricovic proposed the VIKOR method to solve decision-making problems with conflicting criteria [59]. In this method, the ranking of the alternatives is influenced by the initial weight of the problem and its closeness to the objective. In the study, many researchers used the VIKOR method to solve multi-objective problems due to its aptness and feasibility. Some are as follows: Ilangkumaran et al. [60–62] used VIKOR along with some hybrid MCDM models to prioritize best treatment for wastewater management. The VIKOR approach was used by Yazdani and Payam [63] to prioritize material selection for MEMS applications. From the above facts, it is evident that the VIKOR model can be used as an effective tool for ranking alternatives [64–66].

The VIKOR method is started with the subsequent form Lp metric:

$$L_{Pj} = \left\{ \sum_{i=1}^{n} \left[\frac{w_i\left(f_i^* - f_{ij}\right)}{\left(f_i^* - f_i^-\right)} \right]^P \right\}^{1/P} \quad 1 \le P \le \infty, j = 1, 2, \ldots, J. \tag{26}$$

The compromising ranking method of VIKOR is given as follows:

Step 1. Matrix Normalization: let X_{ij} be the evaluation matrix with values of the jth alternatives and ith criteria, and then, the normalized matrix f_{ij} is calculated using

$$f_{ij} = \frac{x_{ij}}{\sqrt{\sum_{i=1}^{m} x_{ij}^2}}, i = 1, 2m; j = 1, 2, n. \tag{27}$$

Step2. *Evaluate the Worst and Best Values* (f^*, f^-): the best and the worst values are given by the following relation:

$$f_i^* = \max_j f_{ij}, f_i^- = \min_j f_{ij.} \tag{28}$$

Step 3. *Calculate the S_j and R_j* Values: the utility measure S_j and regret measure R_j are determined using the relation:

$$S_j = \frac{\sum_{i=1}^{n} w_i\left(f_i^* - f_{ij}\right)}{\left(f_i^* - f_i^-\right)}, \tag{29}$$

$$R_j = \max_i \left[\frac{\left(f_i^* - f_{ij}\right)}{\left(f_i^* - f_i^-\right)} \right]. m \tag{30}$$

Step 4. *Compute the VIKOR Index*: the VIKOR index value Q_j is calculated using

$$Q_j = \frac{v\left(S_j - S^*\right)}{\left(S^- - S^*\right)} + \frac{(1-v)\left(R_j - R^*\right)}{\left(R^- - R^*\right)}, \tag{31}$$

where

$$S* = \min_j S_j, S^- = \max_j S_j, R* = \min_j R_j, R^- = \max_j R_j. \tag{32}$$

Here, $v = 0.5$.

Step 5. *Rank the Alternatives*: the option with the lowest VIKOR index is chosen as the best value.

5. Result and Discussion

From the study [49], it is observed that the modification in peripheral geometry of TT in a smooth tube tends to increase the friction factor, but in terms of the Nusselt number, only a minor improvement is found. The current research looks at the effect of WCTT in grooved tubes. From experimental results, it is observed that different geometrical and operating parameters expose their unique influence on heat transfer, pressure drop, performance enhancement ratio, and rational efficiency. The effects of these parameters are conversed as follows.

Table 3: Fuzzy numbers' membership function.

Scale of linguistic importance	Fuzzy number	(L, M, U)-TFN	$(1/U, 1/M, 1/L)$: reciprocal of TFN
Equally: important	M1	(1, 1, 1)	(1, 1, 1)
Equally: moderate important	M2	(1, 2, 3)	(0.33, 0.5, 1)
Weakly: important	M3	(2, 3, 4)	(0.25, 00.33, 0.5)
Moderate: important	M4	(3, 4, 5)	(0.2, 0.25, 0.33)
Moderately: strong important	M5	(4, 5, 6)	(0.16, 0.2, 0.25)
Strongly: important	M6	(5, 6, 7)	(0.14, 0.16, 0.2)
Very strongly: important	M7	(6, 7, 8)	(0.12, 0.14, 0.16)
Very strongly: extreme important	M8	(7, 8, 9)	(0.11, 0.12, 0.14)
Absolutely: important	M9	(8, 9, 10)	(0.10, 0.11, 0.12)

Table 4: Random consistency index.

No.	1	2	3	4	5	6	7	8	9	10
RCI	0	0	0.52	0.89	1.11	1.25	1.35	1.40	1.45	1.49

5.1. Validation Conventional System. To validate the system's reliability, the plain tube result is compared to the result obtained from the standard correlations given in equations (33) to (36). Once the system's consistency is established, the plain tube heat exchanger results are recorded and compared to the standard correlation results (shown in Figure 7). The results showed that the thermal and flow performance of the plain tube agreed well with the standard correlation in the range of 5% to 8%, respectively. As a result, the results show that the experimental facility and measurement techniques are reliable. The plain tube results are used in upcoming calculations.

Convective heat transfer correlations—Dittus–Boelter correlation is as follows:

$$Nu = 0.023\mathrm{Re}^{0.8}\,\mathrm{Pr}^{0.3} \quad for Re > 10,000. \tag{33}$$

Gnielinski correlation is as follows:

$$Nu = \frac{(f/8)(\mathrm{Re} - 1000)\mathrm{Pr}}{1 + 12.7(f/8)^{0.5}\left(\mathrm{Pr}^{0.33} - 1\right)} \quad for 3000 < Re < 500,000. \tag{34}$$

Correlations for the friction factor—correlation of Blasius is as follows:

$$f = 0.316\mathrm{Re}^{-.025} \quad for Re < 20,000. \tag{35}$$

Petukhov correlation is as follows:

$$f = (0.790 \quad \ln \mathrm{Re} - 1.64)^{-2} \quad for 3000 < Re < 500,000. \tag{36}$$

5.2. Heat Transfer Investigation of WCTT Insert. The effect of twist ratio (y) on heat transfer features in the grooved tube fitted with WCTT is presented in Figure 8. From Figure 8(a), it is observed that the Nusselt number (Nu) of the tube increases with an increase in Reynolds number and decreases in twist ratio. The WCTT having the value of $y = 3.5$ provides maximum heat transfer compared with the other twist ratios. This eddy flow generated by the TTs provides better flow mixing between core and wall of the tube, (2) strong turbulence and vortices near the W-cut region lead to thermal boundary layer destruction, and (3) in addition, the groove in tube causes flow separation, and reattachment and recirculation of water result in effective fluid mixing. The abovementioned flow phenomenon stimulates an increase in the turbulent intensity and tangential turbulent fluctuation, which affects the hydrodynamic and thermal boundary layer and therefore increases the heat transfer of the tube. Over the range studied, the WCTT in grooved tube with $y = 3.5$ provides the mean Nusselt number of about 12%, 20%, and 48% higher than those in the grooved tube with twist ratio of $y = 5.3$ and $y = 6.5$, and plain tube, respectively.

Similarly, the Nu ratio decreases with increasing Reynolds number in all cases, indicating that at lower Reynolds numbers, the flow cannot generate high turbulence on its own, and thus, introducing TT generates secondary swirl on fluid flow and increases heat transfer. At higher Reynolds numbers, the grooved tube itself creates a massive secondary swirl, and hence, the impact of TT becomes less effective. As expected, the Nu ratio of WCTT in the grooved tube compared with the simple tube is always greater than unity. From Figure 8(b), it is obvious that the Nu ratio of the WCTT in the grooved tube is approximately 2–2.5 times higher than in the simple grooved tube and approximately 3.0–3.4 times higher than in the simple tube.

Further, the heat transfer is also governed by the WR of the tape, as shown in Figure 8(a). It is observed that the effect of WR at a higher range yields a larger value of the Nusselt number compared with the smaller one. This is due to the effect of augmented eddies and vorticities behind the cut, which results in the promotion of turbulent intensity and fluid mixing and additionally increases the heat transfer rate. Figure 8 shows that the mean Nusselt number obtained using a W-cut insert in a grooved tube at WR = 0.6 and $y = 3.5$, 5.3, and 6.4 is 2.08%, 2.13%, and 2.17% greater than the grooved inner tube at the same condition, WR = 0.4.

5.3. Friction Factor Characteristics of W-Cut TT Insert. Figure 9 depicts the magnitude of friction with change in mass flow rate of working fluid passed inside the grooved tube fitted with WCTT and plain tube. It is observed that the friction factor followed the decreasing trend with rise in Reynolds number and showed supremacy at lower twist ratio ($y = 3.5$) compared with that of higher twist ratios

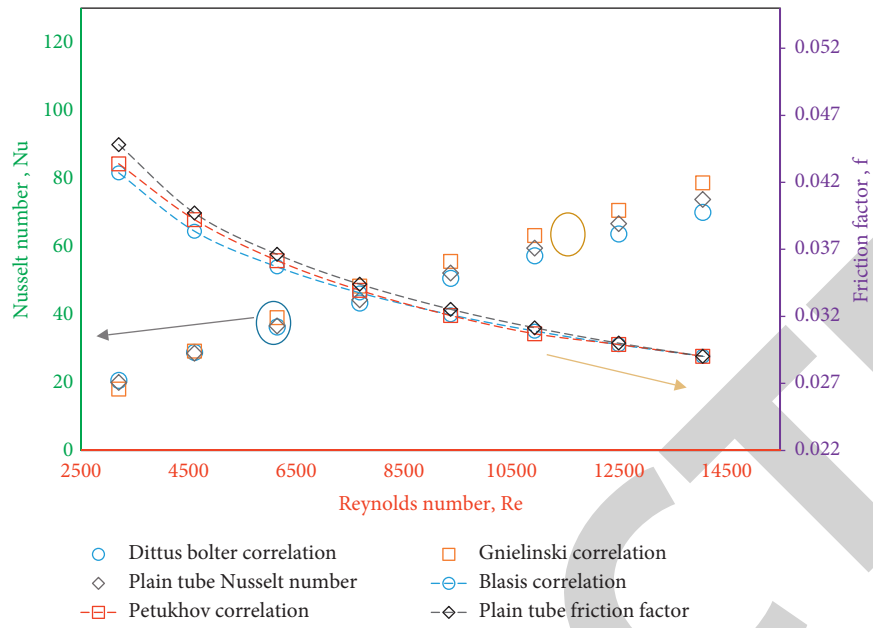

Figure 7: Validation of the plain tube.

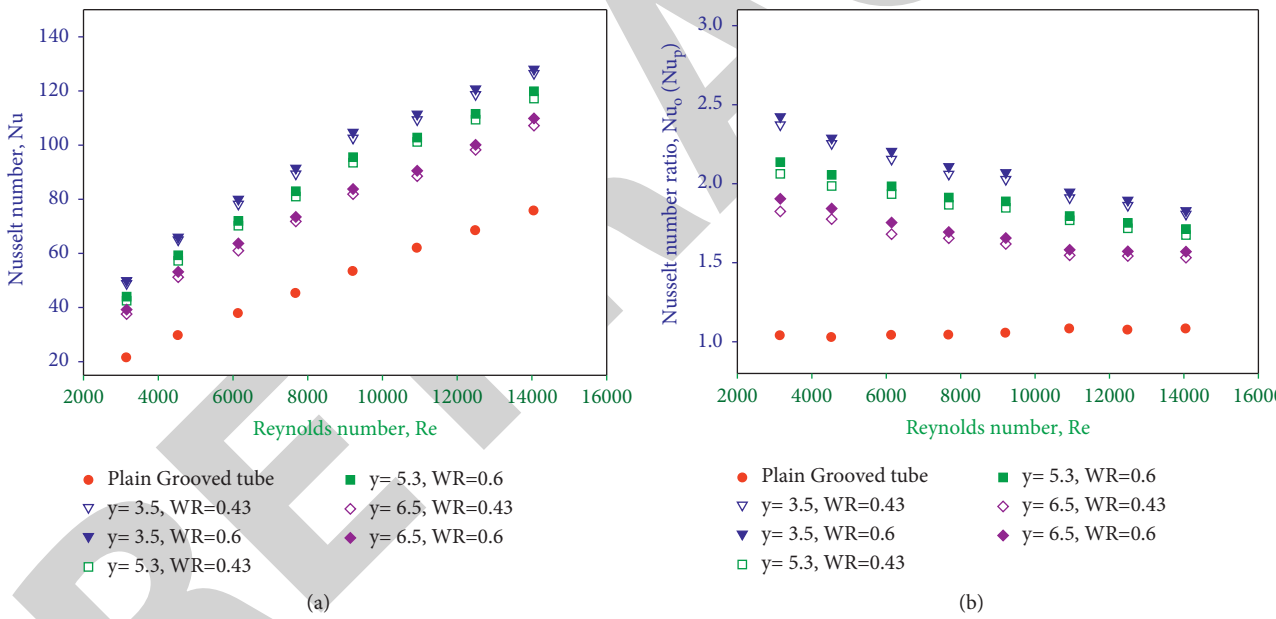

Figure 8: Nusselt number of WCTT: (a) Nu vs. Re. (b) Nu_o/Nu_p vs. Re.

($y = 5.3$ and 6.5). This is due to the effect of secondary flow generated by the WCTTs. At lower twist ratio, the turbulence intensity near the wall increases, which augments the fluid friction. In addition, the lower twist ratio TTs blocks the fluid passage in large volume and increases the surface contact, which results in increased static pressure. Also, the eddies and vortices made by W-cut create extensive friction loss that is normally negligible in case of plain tubes. From the graph, it is clear that the friction factor of the grooved tube with WCTT at $y = 3.5$ is 1.14 and 1.26 times higher than the given tube with $y = 5.3$ and 6.5, consecutively, and 4.5 times greater as compared with plain tube.

Figures 9(a) and 9(b) illustrate the friction factor ratio (f_o/f_P) of WCTT with different twist ratios (y) and width ratios (WRs). The result exposed that the friction factor nature increases with the rise in the Reynolds number. Qualitatively, the pressure loss generated by the WCTT is directly related to the results of the heat transfer discussed in Section 5.2 because an effective heat transfer is caused by the strong turbulence in boundary layer, which concurrently increases the interaction of pressure force with inertia force and thus enhances the dynamic pressure loss. At smaller twist ratio ($y = 3.5$), the friction factor ratio of WCTT is substantially higher than those associated with larger twist

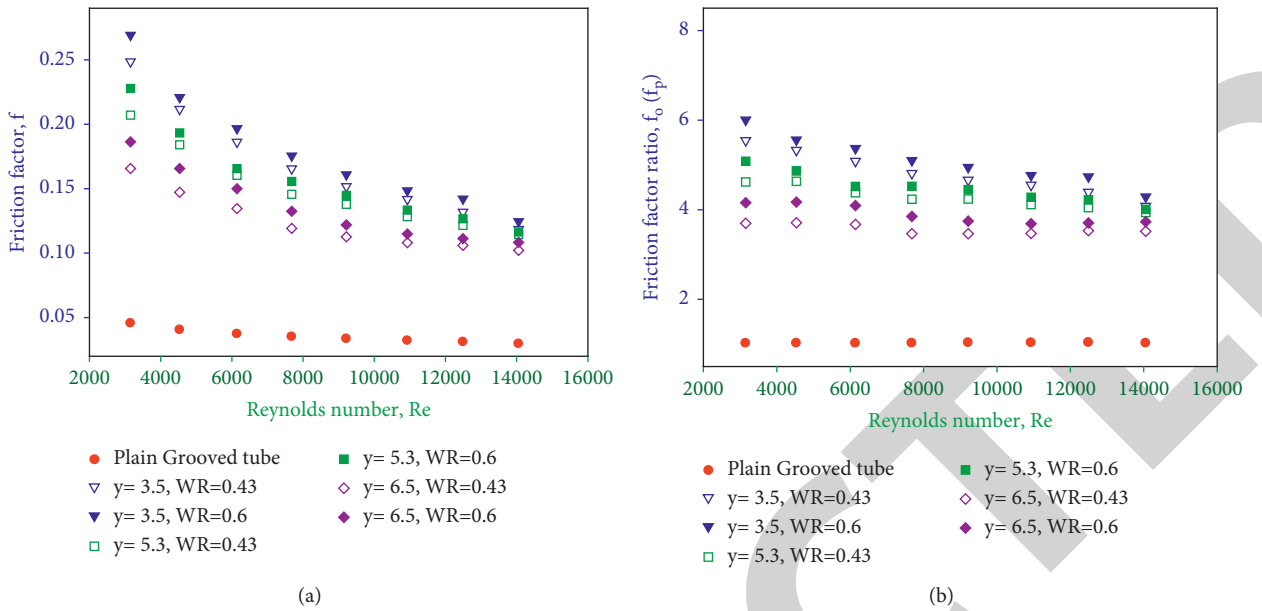

Figure 9: Friction factor of W-cut insert: (a) f vs. Re. (b) f_o/f_p vs. Re.

ratio ($y = 5.3$ and 6.5), which are, respectively, in range of 1.10–1.45 times and about 4.95 times as improved with the conventional system.

The effect of width ratio (WR) on friction factor follows the same trend as the Nusselt number, whereas the friction factor increases with rise in width ratio. For the present range, the mean friction factor of WCTTs with WR of 0.4 at $y = 3.5$, 5.3, and 6.4 is higher than that caused by the use of W-cut insert at WR of 0.6 for given twist ratio by around 5%, 6%, and 8%, respectively.

5.4. Performance Enhancement Ratio. An equal pumping power comparison is attained to evaluate the heat transfer efficiency in terms of PER of the grooved tube fitted with WCTT. The variation of PER with Reynolds number for WCTT at various twist ratios (y) and width ratios is depicted in Figure 10. In all cases, the value of PER decreases with an increase in the Reynolds number. Also, at a given Reynolds number, the PER of the tube tends to increase with a decrease in y and WR. In all of the above cases, the PER shows how this tape helps save energy, and it also shows how the heat transfer ratio affects the friction penalty.

From the figure, it is observed that the mean enhancement ratio of the grooved tube with WCTT at $y = 3.5$ is 1.05 times, 1.5 times, and 2.08 times higher than the grooved tube with $y = 5.3$ and 6.4 and plain grooved tube, respectively. In addition, the WCTT at WR of 0.45 gives a maximum enhancement ratio and is about 0.9–1.4 times higher than the tape with WR of 0.6. This is due to the effect of added pressure drop at higher WR. Hence, it is concluded that the superior performance can be obtained by lower twist ratio and width ratio. However, the above result cannot be optimum, as the pressure drop reaches extreme at this condition. To overcome this problem, MOO techniques are used in this work, to find the optimum results. The

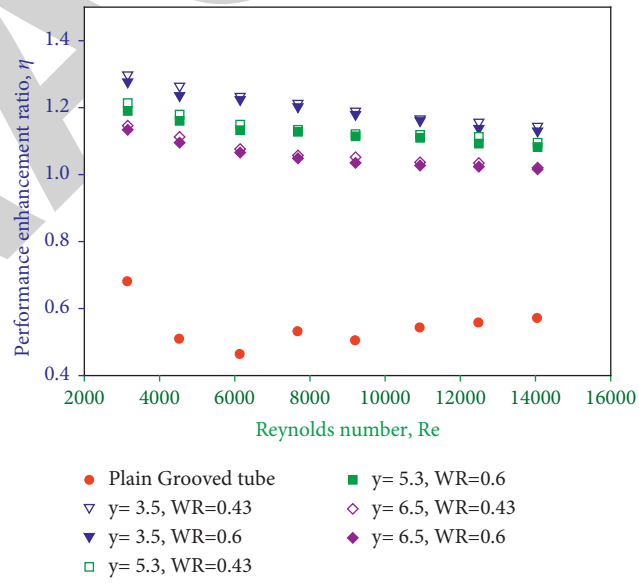

Figure 10: Performance enhancement ratio (η_1) vs. Reynolds number (Re).

parameters such as twist ratio and width ratio of TTs along with the Reynolds number play a major role in selecting optimum thermal performance conditions.

5.5. Rational Analysis of Exergy. The exergetic efficiency of WCTT with various geometries is discussed in this segment. Figure 11 shows the exergy efficiency of the inserts as a function of Reynolds number for various twist ratios and width ratios. When compared to plain grooved tube, the combined effect of WCTTs with grooved tube demonstrated superior rational exergy efficiency. W-cut causes stronger eddies and vortices, which increases decayed boundary layer

thickness and turbulent intensity near the walls, increasing exergetic efficiency. The graph clearly shows that the rational exergetic efficiency of the WCTT with lower twist ratio ($y = 3.5$) outperformed the inserts with higher twist ratio ($y = 5.3$ and 6.5), respectively, by 1.04 and 1.10 times. Aside from that, the width ratio, like the PER discussed in Section 5.4, has an effect on rational exergy efficiency. It is difficult to choose the best because its performance in terms of width ratio is contradictory. As a result, the MOO technique is used in this study to achieve the best results.

5.6. Empirical Correlation. The empirical correlation for Nusselt number, friction factor, performance enhancement ratio, and rational efficiency of the grooved tube with WCTT was developed, as a function of tape geometry (y and WR) and Reynolds number using the least-squares regression analysis. The empirical correlations are as follows:

$$Nu = 0.493\mathrm{Re}^{0.635} y^{-0.33} (Wr)^{0.079}, \quad (37)$$

$$f = 12.3\mathrm{Re}^{-0.401} y^{-0.429} (\mathrm{W_r})^{0.21}, \quad (38)$$

$$\eta_I = 2.81\mathrm{Re}^{-0.071} y^{-0.191} (W_r)^{-0.0384}, \quad (39)$$

$$\eta_{II} = 1.69\mathrm{Re}^{-0.095} y^{-0.1041} (W_r)^{0.06}. \quad (40)$$

Figures 12(a) to 12(d) depict the predicted data of Nusselt number, friction factor, performance enhancement ratio, and rational efficiency from the above correlations (equations 37–(40)) in comparison with those obtained from the experimental data. Apparently, the predicted data are in good concordance with the experimental data with the discrepancy of ±4%, ±7%,± 3%, and ±2% for Nu, f, η_I, and η_{II}, respectively.

6. Optimization Results

From the above experimental study, it is clear that the effects of individual geometric variables on thermal and exergetic efficiency are considered one at a time, but the effects of compound variables are not taken into consideration. It is quite difficult to estimate the optimal working parameter of the WCTT using experimental results, and further, this study has two incompatible objectives (Nu and f). Hence, it is proposed to carry out multi-objective optimization (MOO) and multi-criteria decision-making (MCDM) techniques to determine the best possible design configuration for maximum performance in a grooved tube fitted with WCTT.

6.1. Optimization Using Multi-Objective Genetic Algorithm. The main objective of this study is to find the optimum working parameters of the grooved tube with WCTT using GA, which leads to the maximization of the Nusselt number and minimization of pressure drop. Owing to conflicting objectives, the negative Nusselt number (−Nu) is taken as defining parameter, such that lower the value of −Nu gives maximum heat transfer.

The multi-objective problem in the optimization of WCTTs is as follows.

Minimization $f(\mathrm{Re}, y, WR) = [-Nu, f]$.

The abovementioned functions are subjected to the parameters in the range of $2000 \le \mathrm{Re} \le 14000$, $3.5 \le y \le 6.4$, and $0.45 \le \mathrm{WR} \le 0.6$. In the given MOO technique, two geometric variables of WCTTs, namely, twist ratio (y) and width ratio (WR), and Reynolds number (Re) are chosen as the design variables. The maximum and minimum bounds of the design variables are shown in Table 5.

In this study, the GA technique is effectively used to determine the optimal Pareto front for the conflicting objectives. The detailed procedure of GA search method to generate optical Pareto front solutions is provided [50]. The parameter setting of GA is given in Table 6. The optimal Pareto front searched by the GA is shown in Figure 13, and their corresponding values are depicted in Table 7. It is clear that the all points in Pareto front are optimal points and they do not have any supremacy over each other. It is also observed that variation from one optimal point to another leads to the improvement of one objective with inimical change in the other. Thus, in this work, to select the optimal design configuration for heat exchanger with WCTT, the multi-objective genetic algorithm is used, in which the η and η_{II} are used to evaluate the heat transfer against the friction factor. The corresponding values of η and η_{II} compared against the two objective functions in optimal Pareto front are illustrated in Figures 14 and 15, respectively. Evidently, the extreme value of η and η_{II} from the figures gives the optimum geometric parameters for the defined problem.

Though the geometric points obtained using Pareto front of MOGA can be taken as the best, one cannot eliminate the remaining solutions, as all the values specified by Pareto front are optimal. Hence, to identify the best operating configuration from the Pareto front set, this study utilizes FAHP-VIKOR model as decision-making tool.

6.2. Optimization Using MCDM. This study utilizes the hybrid MCDM model to identify the best operating configuration from the set of Pareto values (taken as alternatives). The performance-defining criteria of the given problem are identified and are given in Table 8. In this phase, hybrid MCDM model, FAHP-TOPSIS, is used to rank the alternatives. Here, FAHP is used to assign weightage for the criteria and VIKOR is used to rank the alternatives.

6.2.1. Calculation of Weightage for Criteria. The weightage of criteria used in the study is calculated using the fuzzy analytical hierarchical process (FAHP) method. The nonconformity values of the alternatives associated with predefined criteria are depicted in Figure 16. Once the hierarchy diagram is framed, the FAHP computes the weights of each criterion by making pairwise comparison with Satty's nine-point scale. The fuzzy pairwise comparison results of the criteria are shown in Table 9. The geometric mean values are computed, and the final pairwise comparison matrix is constructed. The weight of each criterion is calculated and tabulated in Table 10 based on the final matrix. Consistency

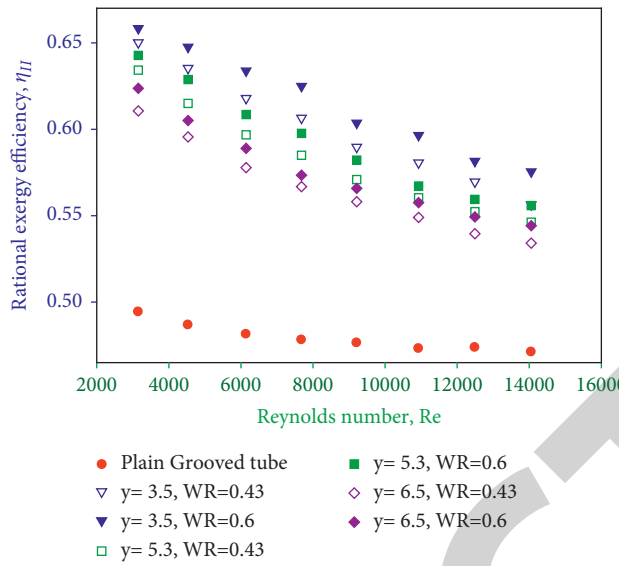

Figure 11: Exergy efficiency (η_{II}) vs. Reynolds number (Re).

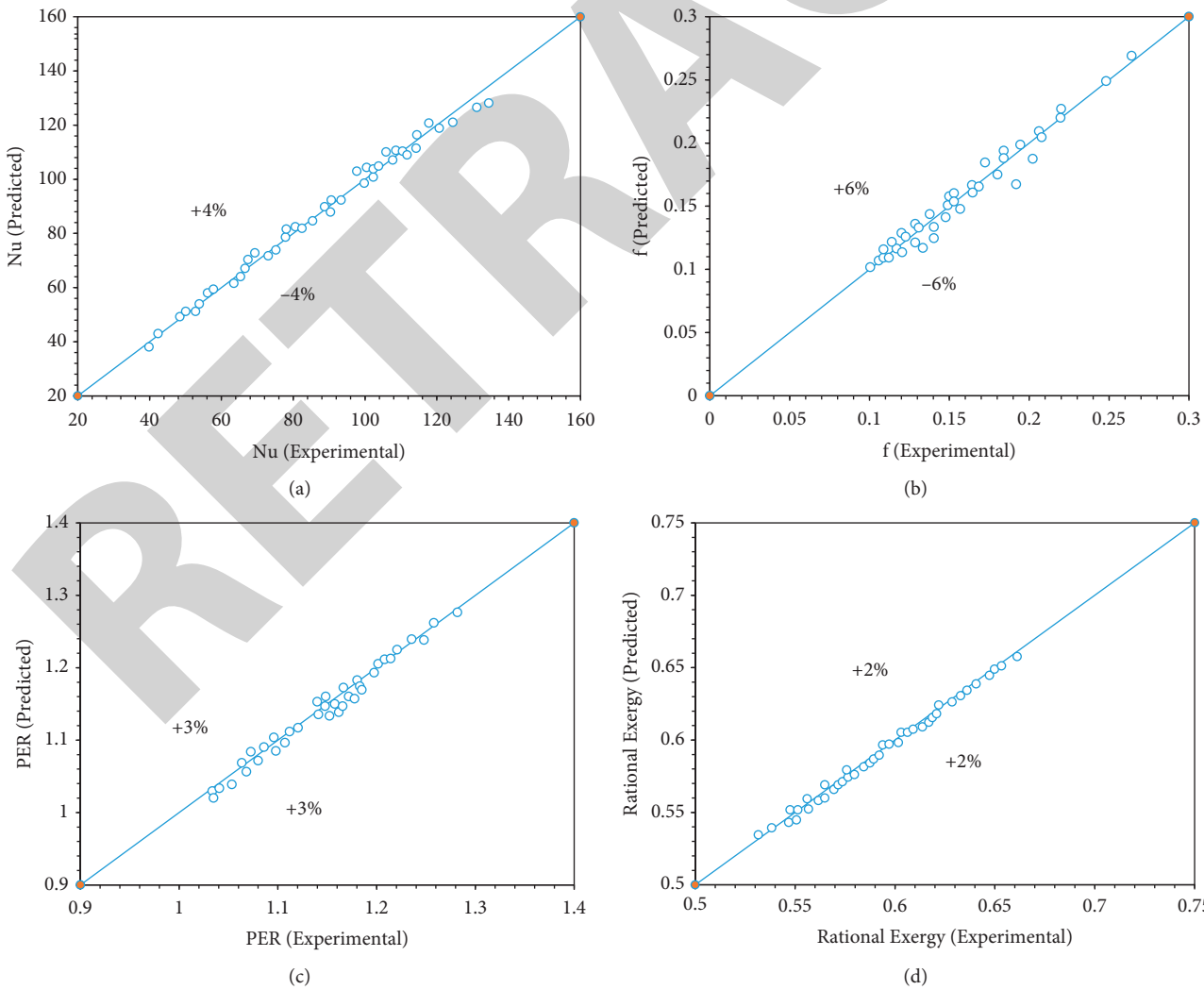

Figure 12: Assessment between the experimental and developed correlation results: (a) Nu, (b) fr, (c) η, (d) η_{II}.

Table 5: Range of design variables and the selected values.

Design variables	Lower bound	Higher bound	Selected values
Twist ratio (y)	3.5	6.4	3.5, 5.3, 6.4
Width ratio (WR)	0.45	0.6	0.45, 0.6
Reynolds number	3000	14000	3000, 4500, 6100, 7600, 9200, 10900, 12500, 14000

Table 6: Parameter setting for GA.

Parameter	Value setting
Population size	100
Pareto front population fraction	0.7
Cross fraction	0.8
Generation	500
Fractional tolerance	10^6

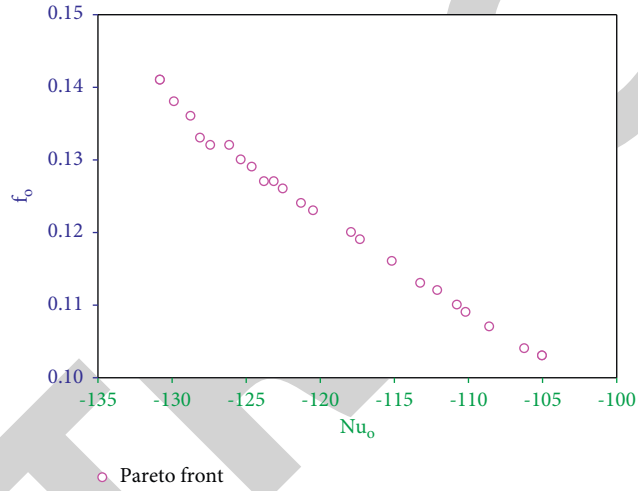

Figure 13: Optimal Pareto front solution.

index (CI) and consistency ratio (CR) values are calculated using equations (28) and (29) to check the consistency of the criteria in the pairwise comparison matrix. The CR value is 0.073, which is less than 0.1, according to the results. As a result, the weights assigned to the criteria are satisfactory and can be used to rank the alternatives.

6.2.2. Ranking the Alternatives. In this section, the VIKOR method is proposed for selecting the optimum design among the list of alternatives. The decision matrix of the stated problem is shown in Table 11, and the values of the decision matrix are normalized using equation (31). The normalized decision matrix values are calculated and tabulated in Table 12. The best and worst values of each criterion are calculated using equation (32) and are depicted in Table 13, followed by the construction of utility measure relation, regret measure relation, and VIKOR index using equations (33)–(35) shown in Table 14. The ranking of the options is prioritized according to the VIKOR index value, as shown in Table 14 and Figure 17. The alternative A4 among the list of 25 alternatives is the most preferred, as it attains the first rank with concern to overall objectives. According to VIKOR index values, the WCTT configuration rankings are as follows: A4 > A11 > A2 > A9 > A21 > A17 > A1 > A24 > A11 > A23 > A7 > A18 > A13 > A10 > A20 > A5 > A19 > A14 > A16 > A22 > A25 > A6 > A15 > A3 > A8. The alternative with twist ratio, $y = 3.55$, width ratio, WR = 0.489, and Reynolds number, Re = 13511, exhibits the optimal formulation.

To validate the optimum configuration, the obtained result is compared with the other inserts from the past under similar working condition. Figure 18 depicted the comparative result of the optimum configuration of WCTT with other inserts. The result showed that the optimum configuration of WCTT showed supremacy over other inserts in the range of 0.5–31.5%, respectively. The WCTT effectively breaks the viscose and thermal boundary layers formulated inside the tubes at turbulent flow conditions. Further, the W-shaped design offers lower flow resistance. This makes the system higher efficient as compared with other configurations of turbulator designs.

Table 7: Optimal configurations of W-cut twisted tapes (Pareto front solutions from GA).

PDAs	Criteria				
	RE	Y	WR	−Nu	f
A1	13509.24	3.585487	0.447139	−127.404	0.132
A2	13509.22	3.544997	0.594741	−130.796	0.141
A3	13520.53	6.396681	0.431835	−105.015	0.103
A4	13510.76	3.550541	0.488913	−128.730	0.136
A5	13513.59	4.584293	0.43714	−117.294	0.119
A6	13518.59	5.788635	0.434234	−108.572	0.107
A7	13511.20	3.894812	0.437794	−123.776	0.127
A8	13520.53	6.396681	0.431835	−105.015	0.103
A9	13509.22	3.544997	0.594741	−130.796	0.141
A10	1351200	4.218427	0.433286	−120.465	0.123
A11	13510.45	3.507667	0.436446	−128.092	0.133
A12	13509.70	3.530505	0.533291	−129.853	0.138
A13	13511.81	4.137216	0.434913	−121.275	0.124
A14	13515.52	5.104409	0.437658	−113.228	0.113
A15	13518.51	6.192659	0.435724	−106.210	0.104
A16	13518.68	5.480163	0.444343	−110.754	0.110
A17	13510.48	3.781659	0.454154	−125.345	0.130
A18	13511.81	4.012216	0.434913	−122.509	0.126
A19	13514.91	4.846300	0.436005	−115.146	0.116
A20	13512.97	4.524871	0.442025	−117.900	0.120
A21	13510.40	3.761377	0.479983	−126.117	0.132
A22	13516.24	5.263390	0.436984	−112.078	0.112
A23	13510.49	3.972317	0.444530	−123.118	0.127
A24	13509.49	3.835487	0.447139	−124.603	0.129
A25	13518.59	5.538635	0.434234	−110.165	0.109

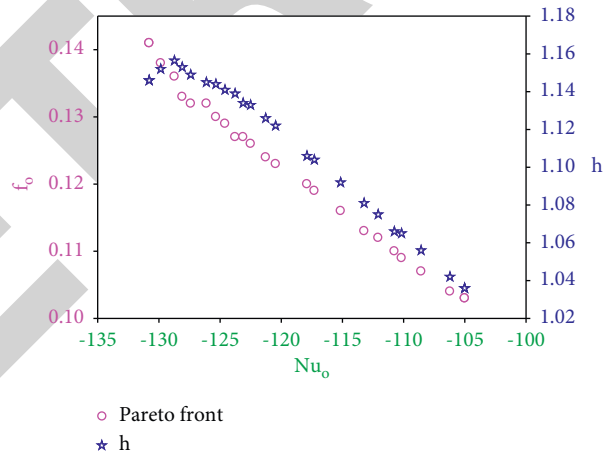

Figure 14: Multi-objective optimization of Pareto front (η).

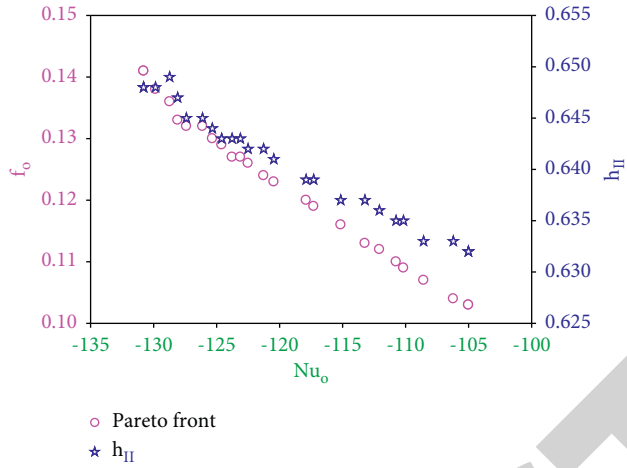

Figure 15: Multi-objective optimization of Pareto front (η_{II}).

Table 8: Details of the different criteria.

Criteria	Notations	Performance implications of different criteria.
Thermal enhancement ratio (TER)	(Nu_o/Nu_p)	C1-higher-the better
Friction enhancement ratio (FER)	(f_o/f_p)	C2-lower-the better
Performance enhancement ratio (PER)	(η_I)	C3-higher-the better
Rational exergy efficiency (REE)	(η_{II})	C4-higher-the better

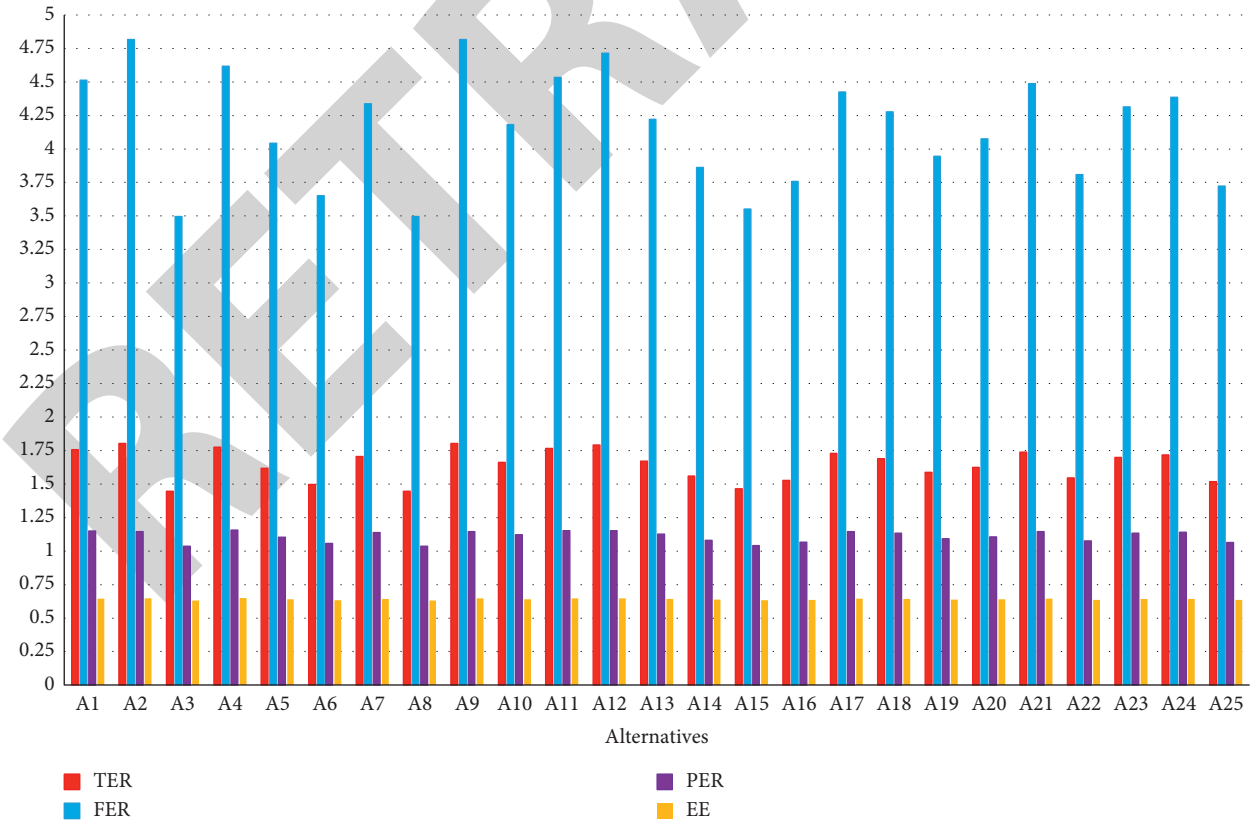

Figure 16: Inconsistency of criteria values with alternatives.

Table 9: Pairwise comparison matrix for criteria.

	TER	FER	PER	REE
TER	(1, 1, 1)	(1, 1, 1)	(0.25, 00.33, 0.5)	(0.25, 00.33, 0.5)
FER	(1, 1, 1)	(1, 1, 1)	(0.25, 00.33, 0.5)	(0.25, 00.33, 0.5)
PER	(2, 3, 4)	(2, 3, 4)	(1, 1, 1)	(00.33, 0.5, 1)
EE	(2, 3, 4)	(2, 3, 4)	(1, 2, 3)	(1, 1, 1)

Table 10: Results obtained with FAHP.

Criteria	Weights	λ_{max}, CI, RCI	CR
TER	0.1198	$\lambda_{max} = 4.201$, CI = 0.0669, RCI = 0.9	0.073
FER	0.1198		
PER	0.3476		
REE	0.4128		

Table 11: Details of alternatives and criteria (decision matrix).

PDAs	Criteria			
	TER	FER	PER	REE
A1	−1.76	4.514	1.149	0.645
A2	−1.8	4.816	1.146	0.648
A3	−1.45	3.495	1.036	0.632
A4	−1.77	4.618	1.157	0.649
A5	−1.62	4.043	1.104	0.639
A6	−1.5	3.652	1.056	0.633
A7	−1.71	4.337	1.139	0.643
A8	−1.45	3.495	1.036	0.632
A9	−1.8	4.816	1.146	0.648
A10	−1.66	4.182	1.122	0.641
A11	−1.77	4.533	1.153	0.647
A12	−1.79	4.715	1.152	0.648
A13	−1.67	4.22	1.126	0.642
A14	−1.56	3.861	1.081	0.637
A15	−1.46	3.551	1.042	0.633
A16	−1.53	3.757	1.066	0.635
A17	−1.73	4.426	1.144	0.644
A18	−1.69	4.276	1.133	0.642
A19	−1.59	3.945	1.092	0.637
A20	−1.63	4.075	1.106	0.639
A21	−1.74	4.488	1.145	0.645
A22	−1.54	3.81	1.075	0.636
A23	−1.7	4.314	1.134	0.643
A24	−1.72	4.385	1.141	0.643
A25	−1.52	3.722	1.065	0.635

Table 12: Weighted normalized decision matrix.

PDAs	Criteria			
	TER	FER	PER	REE
A1	0.1041	0.0924	0.0033	0.2086
A2	0.1198	0.1198	0.0245	0.0442
A3	0.0000	0.0000	0.3476	0.4128
A4	0.1102	0.1019	0.0000	0.0000
A5	0.0571	0.0497	0.1482	0.3071
A6	0.0165	0.0143	0.2894	0.3784
A7	0.0872	0.0764	0.0454	0.2621
A8	0.0000	0.0000	0.3476	0.4128
A9	0.1198	0.1198	0.0245	0.0442

Table 12: Continued.

PDAs	Criteria			
	TER	FER	PER	REE
A10	0.0718	0.0623	0.0949	0.2985
A11	0.1072	0.0942	0.0033	0.2394
A12	0.1154	0.1107	0.0076	0.0108
A13	0.0756	0.0658	0.0831	0.2878
A14	0.0382	0.0332	0.2145	0.3335
A15	0.0056	0.0051	0.3296	0.3907
A16	0.0266	0.0238	0.2594	0.3299
A17	0.0945	0.0845	0.0312	0.1993
A18	0.0813	0.0709	0.0636	0.2798
A19	0.0471	0.0408	0.1823	0.3256
A20	0.0599	0.0526	0.1415	0.2870
A21	0.0981	0.0901	0.0349	0.1147
A22	0.0328	0.0285	0.2330	0.3439
A23	0.0842	0.0743	0.0600	0.2443
A24	0.0911	0.0807	0.0383	0.2262
A25	0.0239	0.0206	0.2630	0.3669

Table 13: Best and worst values of criteria.

	TER	FER	PER	EE
Best value (f_i^*)	1.80	4.82	1.16	0.65
Worst value (f_i^*)	1.45	3.50	1.04	0.63

Table 14: S_i, R_i, and Q_i values and ranking of alternatives using VIKOR.

PDAs	Criteria			
	S_i	R_i	Q_i	Rank
A1	0.41	0.21	0.0750	4
A2	0.31	0.12	0.0768	3
A3	0.76	0.41	1.0000	24
A4	0.21	0.11	0.0076	1
A5	0.56	0.31	0.4878	16
A6	0.70	0.38	0.9067	22
A7	0.47	0.26	0.2029	10
A8	0.76	0.41	1.0000	25
A9	0.31	0.12	0.0768	6
A10	0.53	0.30	0.3441	14
A11	0.44	0.24	0.0304	2
A12	0.24	0.12	0.0480	3
A13	0.51	0.29	0.2822	13
A14	0.62	0.33	0.6411	18
A15	0.73	0.39	0.9341	23
A16	0.64	0.33	0.7791	20
A17	0.41	0.20	0.1397	8
A18	0.50	0.28	0.2686	12
A19	0.60	0.33	0.6196	17
A20	0.54	0.29	0.4841	15
A21	0.34	0.11	0.0849	7
A22	0.64	0.34	0.7070	19
A23	0.46	0.24	0.2129	11
A24	0.44	0.23	0.1994	9
A25	0.67	0.37	0.7807	21

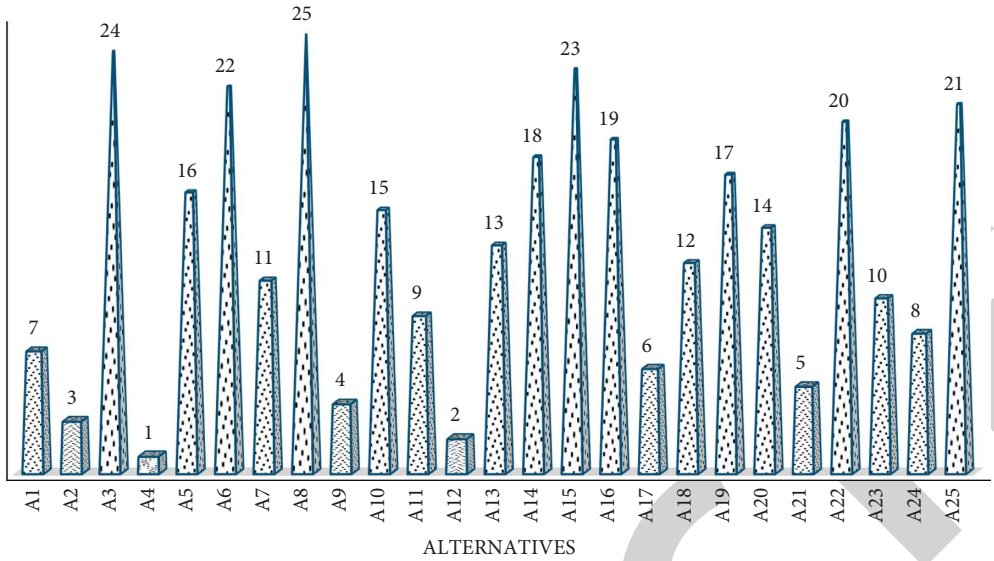

Figure 17: Ranking of alternatives.

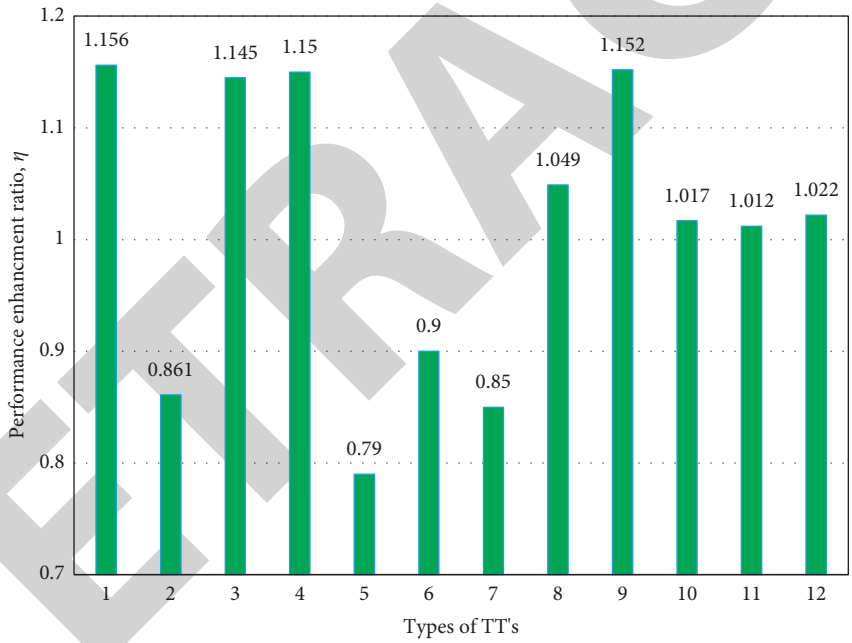

1. Present tape (W-cut TT)
2. Large/small twin TT [26]
3. TT Consisting of Wire-nails [6]
4. Horizontal wing-cut TT [5]
5. Twisted tape inserts [18]
6. Helically TT with alternate axis [23]
7. cross hollow TT [16]
8. Dual TT [16]
9. centre-cleared TT [15]
10. Tapered TT [5]
11. Peripherally cut dual TT [12]
12. perforated helical TT [19]

Figure 18: Performance comparison of optimal configuration WCTT with former tapes.

7. Conclusions

To ascertain the best performance configuration of WCTT, the twist ratio, width ratio, and Reynolds number parameters are to be considered, which consists of conflicting objectives with a major focus on meeting enhanced heat transfer. Therefore, an effective optimization concept is essential to resolve the problem. This work uses optimization tools such as genetic algorithm and FAHP-VIKOR on experimental results with varying parameters to identify the best one. Initially, the effect of grooved tube with WCTT is carried out to show the deviance of objectives with the variation of parameters. Then, the set of optimal solutions for the conflicting objectives is identified using multi-objective GA. Finally, the best optimal solution is obtained using the FAHP-VIKOR model. The results of the current work are as follows.

(i) The Nusselt number increases with rise in Reynolds number and width ratio and with decrease in twist ratio. The Nusselt number of the grooved tube with WCTT showed 44–56% higher heat transfer rate than plain tube.

(ii) The friction factor increases with a decrease in Reynolds number and twist ratio and with the increase in width ratio. The rise in friction factor is noticed for the grooved tube fitted WCTT than the plain tube of about 71–78%.

(iii) The performance enhancement ratio of WCTT is in the range of 1.02–1.30 for the given working conditions, and it raises with the reduction in twist tape ratio, width ratio, and Reynolds number.

(iv) The rational exergy efficiency increases with the increase in width ratio, in addition with the reduction in twist tape ratio and flow rate. The mean exergy efficiency of the grooved tube with WCTT is about 1.17–1.28 times higher than the plain tube.

(v) The empirical correlation for the Nusselt number, friction factor, performance enhancement ratio, and rational efficiency was developed, and they showed the discrepancy of ±3.5%, ±6%, ±2%, and ±1.5%, respectively.

(vi) As the design parameters such as twist ratio, width ratio, and Reynolds number strongly influence the overall system performance and to optimize the best working configuration, the integrated GA and FAHP-VIKOR optimization tools are used.

(vii) The genetic algorithm is used to optimize the given data and provides the set of optimal Pareto front solutions. This optimal design leads to trade-off between Nu and f, which results in the use of multi-objective genetic algorithm.

(viii) As all the given solutions of Pareto front were optimum and in the necessity to prioritize the best, the FAHP-VIKOR model is evaluated.

(ix) The order of criteria that dominate the VIKOR index is REE > PER > FER > TER. These criteria are determined to optimize the overall performance of grooved tube heat exchanger employing WCTTs. These performance criteria weights are calculated using FAHP, and their contribution ratio of order is 41.26%, 34.76%, 11.98%, and 11.98%, respectively.

(x) The optimal formulation is A4 with twist ratio (y): 3.55, width ratio (WR): 0.488, and Reynolds number (Re): 13511, which gives outcomes of thermal enhancement ratio (Nu_o/Nu_p): 1.177; friction enhancement ratio (f_o/f_p): 4.62; performance enhancement ratio: 1.15; and exergy efficiency: 0.649.

Nomenclature

A: Surface area of heat exchanger (m^2)
C_p: Specific heat of hot fluid (J/kg·K)
d_i: Inner diameter of heat exchanger's inner tube (m)
E^{out}: Exergy output (W)
E_{useful}: Useful exergy output (W)
E: Qualitative exergy of HX (W)
f_o/f_p: Ratio of friction factor for HX
I': Exergy lost (W)
L: Heat exchanger tube length (m)
Nu: Nusselt number
ΔP: Drop in pressure due to fluid friction
Q: Energy transfer rate (W)
S: Entropy
WR: Width ratio
d_o: Outer diameter of heat exchanger's inner tube (m)
d_h: Hydraulic diameter (m)
E^{in}: Exergy input (W)
E_{waste}: External exergy loss (W)
f: Fluid friction factor of HX
h: Heat transfer coefficient (W/mK)
H: Tape pitch distance (m)
K: Thermal conductivity (W/mK)
m: Fluid mass flow rate (kg/s)
Nu_o/Nu_p: Nusselt number enhancement ratio
P_r: Prandtl number
Re: Reynolds number
T_o: Ambient temperature (°C)
Y: Twist tape ratio

Greek symbols.

η_{II}: Exergy efficiency
ν: Dynamic viscosity (kg/ms)
ρ: Density (kg/m^3)
μ: Kinematic viscosity (m^2/s)
η: Performance enhancement ratio

Abbreviations

TT: Twisted tape
PER: Performance enhancement ratio
WCTT: W-cut twisted tape

Subscripts

O: Exit or outlet
C: Cold
Stream: Material stream
I: Inlet
H: Hot
Q: Heat stream.

Data Availability

The data used to support the findings of this study are included within the article.

Conflicts of Interest

The authors declare that there are no conflicts of interest regarding the publication of this article.

References

[1] C. N. Kumar and P. Murugesan, "Review on twisted tapes heat transfer enhancement," *International Journal of Scientific Engineering and Research*, vol. 3, no. 4, pp. 726–734, 2012.

[2] S. Tamna, Y. Kaewkohkiat, S. Skullong, and P. Promvonge, "Heat transfer enhancement in tubular heat exchanger with double V-ribbed twisted-tapes," *Case Studies in Thermal Engineering*, vol. 7, pp. 14–24, 2016.

[3] P. Murugesan, K. Mayilsamy, and S. Suresh, "Heat transfer in a tube fitted with vertical and horizontal wing-cut twisted tapes," *Experimental Heat Transfer*, vol. 25, no. 1, pp. 30–47, 2012.

[4] A. Hasanpour, M. Farhadi, and K. Sedighi, "Experimental heat transfer and pressure drop study on typical, perforated, V-cut and U-cut twisted tapes in a helically corrugated heat exchanger," *International Communications in Heat and Mass Transfer*, vol. 71, pp. 126–136, 2016.

[5] N. Piriyarungrod, S. Eiamsa-ard, C. Thianpong, M. Pimsarn, and K. Nanan, "Heat transfer enhancement by tapered twisted tape inserts," *Chemical Engineering and Processing: Process Intensification*, vol. 96, pp. 62–71, 2015.

[6] P. Murugesan, K. Mayilsamy, and S. Suresh, "Heat transfer and friction factor studies in a circular tube fitted with twisted tape consisting of wire-nails," *Chinese Journal of Chemical Engineering*, vol. 18, no. 6, pp. 1038–1042, 2010.

[7] S. Gunes and E. Karakaya, "Thermal characteristics in a tube with loose-fit perforated twisted tapes," *Heat Transfer Engineering*, vol. 36, no. 18, pp. 1504–1517, 2015.

[8] M. Jafaryar, M. Sheikholeslami, Z. Li, and R. Moradi, "Nanofluid turbulent flow in a pipe under the effect of twisted tape with alternate axis," *Journal of Thermal Analysis and Calorimetry*, vol. 135, no. 1, pp. 305–323, 2018.

[9] A. A. Giniyatullin, S. E. Tarasevich, and A. B. YakovlevYakovlev, "Heat transfer in a water flow in tubes with ribbed twisted tape inserts," *High Temperature*, vol. 56, no. 2, pp. 302–305, 2018.

[10] A. V. Shishkin and S. E. Tarasevich, "Heat transfer and structure of flow at boiling of refrigerant R134a in channels with inserts in the form of finned twisted tape," *Journal of Physics: Conference Series*, vol. 980, no. 1, Article ID 012012, 2018, March.

[11] Y. He, L. Liu, P. Li, and L. Ma, "Experimental study on heat transfer enhancement characteristics of tube with cross hollow twisted tape inserts," *Applied Thermal Engineering*, vol. 131, pp. 743–749, 2018.

[12] W. Changcharoen, P. Somravysin, and S. Eiamsa-ard, "Thermal and fluid flow characteristics in a tube equipped with peripherally-cut dual twisted tapes," *Open Engineering*, vol. 5, no. 1, 2014.

[13] A. Saravanan, J. S. Senthilkumaar, and S. Jaisankar, "Performance assessment in V-trough solar water heater fitted with square and V-cut twisted tape inserts," *Applied Thermal Engineering*, vol. 102, pp. 476–486, 2016.

[14] K. Yongsiri, C. Thianpong, K. Nanan, and S. Eiamsa-ard, "Thermal performance enhancement in tubes using helically twisted tape with alternate axis inserts," *Thermophysics and Aeromechanics*, vol. 23, no. 1, pp. 69–81, 2016.

[15] S. Pal and S. K. Saha, "Laminar flow and heat transfer through a circular tube having integral transverse corrugations and fitted with centre-cleared twisted-tape," *Experimental Thermal and Fluid Science*, vol. 57, pp. 388–395, 2014.

[16] W. Changcharoen, P. Samruaisin, P. Eiamsa-ard, and S. Eiamsa-ard, "Heat transfer characteristics of decaying swirl flow through a circular tube with co/counter dual twisted-tape swirl generators," *Thermophysics and Aeromechanics*, vol. 23, no. 4, pp. 523–536, 2016.

[17] B. Salam, S. Biswas, S. Saha, and M. M. K. Bhuiya, "Heat transfer enhancement in a tube using rectangular-cut twisted tape insert," *Procedia Engineering*, vol. 56, pp. 96–103, 2013.

[18] S. Chamoli, R. Lu, and P. Yu, "Thermal characteristic of a turbulent flow through a circular tube fitted with perforated vortex generator inserts," *Applied Thermal Engineering*, vol. 121, pp. 1117–1134, 2017.

[19] K. Nanan, C. Thianpong, P. Promvonge, and S. Eiamsa-ard, "Investigation of heat transfer enhancement by perforated helical twisted-tapes," *International Communications in Heat and Mass Transfer*, vol. 52, pp. 106–112, 2014.

[20] B. Kumar, A. K. Patil, S. Jain, and M. Kumar, "Effects of double V cuts in perforated twisted tape insert: an experimental study," *Heat Transfer Engineering*, vol. 41, no. 17, pp. 1473–1484, 2020.

[21] C. Man, X. Lv, J. Hu, P. Sun, and Y. Tang, "Experimental study on effect of heat transfer enhancement for single-phase forced convective flow with twisted tape inserts," *International Journal of Heat and Mass Transfer*, vol. 106, pp. 877–883, 2017.

[22] A. T. Wijayanta, M. Aziz, and M. Aziz, "Heat transfer augmentation of internal flow using twisted tape insert in turbulent flow," *Heat Transfer Engineering*, vol. 41, no. 14, pp. 1288–1300, 2020.

[23] A. T. Wijayanta, B. Pranowo, M. Mirmanto, B. Kristiawan, and M. Aziz, "Internal flow in an enhanced tube having square-cut twisted tape insert," *Energies*, vol. 12, no. 2, p. 306, 2019.

[24] I. Yaningsih, A. T. Wijayanta, T. Miyazaki, and S. Koyama, "V-cut twisted tape insert effect on heat transfer enhancement of single phase turbulent flow heat exchanger," in *AIP Conference Proceedings*vol. 1931, no. 1, AIP Publishing LLC, Article ID 030038, 2018.

[25] I. Yaningsih and A. T. Wijayanta, "Concentric tube heat exchanger installed by twisted tapes using various wings with

alternate axes," in *AIP Conference Proceedings*vol. 1788, no. 1, AIP Publishing LLC, Article ID 030005, 2017.

[26] I. Yaningsih, T. Istanto, and A. T. Wijayanta, "Experimental study of heat transfer enhancement in a concentric double pipe heat exchanger with different axial pitch ratio of perforated twisted tape inserts," *AIP Conference Proceedings*, AIP Publishing LLC, vol. 1717, no. 1, Article ID 030012, 2016.

[27] P. Bharadwaj, A. D. Khondge, and A. W. Date, "Heat transfer and pressure drop in a spirally grooved tube with twisted tape insert," *International Journal of Heat and Mass Transfer*, vol. 52, no. 7-8, pp. 1938–1944, 2009.

[28] D. G. Kumbhar D.G. and N. K. Sane N.K., "Exploring heat transfer and friction factor performance of a dimpled tube equipped with regularly spaced twisted tape inserts," *Procedia Engineering*, vol. 127, pp. 1142–1149, 2015.

[29] Y. Hong, J. Du, and S. Wang, "Experimental heat transfer and flow characteristics in a spiral grooved tube with overlapped large/small twin twisted tapes," *International Journal of Heat and Mass Transfer*, vol. 106, pp. 1178–1190, 2017.

[30] A. Verma, M. Kumar, and A. K. Patil, "Enhanced heat transfer and frictional losses in heat exchanger tube with modified helical coiled inserts," *Heat and Mass Transfer*, vol. 54, no. 10, pp. 3137–3150, 2018.

[31] P. Promvonge, S. Pethkool, M. Pimsarn, and C. ThianpongThianpong, "Heat transfer augmentation in a helical-ribbed tube with double twisted tape inserts," *International Communications in Heat and Mass Transfer*, vol. 39, no. 7, pp. 953–959, 2012.

[32] Y. Hong, X. Deng, and L. Zhang, "3D numerical study on compound heat transfer enhancement of converging-diverging tubes equipped with twin twisted Tapes," *Chinese Journal of Chemical Engineering*, vol. 20, no. 3, pp. 589–601, 2012.

[33] Y. Zhou, J. Yu, and X. Chen, "Thermodynamic optimization analysis of a tube-in-tube helically coiled heat exchanger for Joule-Thomson refrigerators," *International Journal of Thermal Sciences*, vol. 58, pp. 151–156, 2012.

[34] V. J. Manoj Praveen, R. Vigneshkumar, N. Karthikeyan, A. Gurumoorthi, R. Vijayakumar, and P. Madhu, "Heat transfer enhancement of air-concrete thermal energy storage system - CFD simulation and experimental validation under transient condition," *Proceedings of the Institution of Mechanical Engineers - Part E: Journal of Process Mechanical Engineering*, vol. 235, no. 5, pp. 1304–1314, 2021.

[35] A. T. Wijayanta, I. Yaningsih, W. E. Juwana, M. Aziz, and T. Miyazaki, "Effect of wing-pitch ratio of double-sided delta-wing tape insert on the improvement of convective heat transfer," *International Journal of Thermal Sciences*, vol. 151, Article ID 106261, 2020.

[36] M. Z. A. Khan, M. Aziz, and A. T. Wijayanta, "Prediction of heat transfer enhancement of delta-wing tape inserts using artificial neural network," *Case Studies in Thermal Engineering*, vol. 27, Article ID 101322, 2021.

[37] A. T. Wijayanta, I. Yaningsih, M. Aziz, T. Miyazaki, and S. Koyama, "Double-sided delta-wing tape inserts to enhance convective heat transfer and fluid flow characteristics of a double-pipe heat exchanger," *Applied Thermal Engineering*, vol. 145, pp. 27–37, 2018.

[38] A. T. Wijayanta, M. Aziz, K. Kariya, and A. Miyara, "Numerical study of heat transfer enhancement of internal flow using double-sided delta-winglet tape insert," *Energies*, vol. 11, no. 11, p. 3170, 2018.

[39] I. Yaningsih, A. T. Wijayanta, T. Miyazaki, and S. Koyama, "Impact of blockage ratio on thermal performance of delta-winglet vortex generators," *Applied Sciences*, vol. 8, no. 2, p. 181, 2018.

[40] A. T. Wijayanta, T. Istanto, K. Kariya, and A. Miyara, "Heat transfer enhancement of internal flow by inserting punched delta winglet vortex generators with various attack angles," *Experimental Thermal and Fluid Science*, vol. 87, pp. 141–148, 2017.

[41] M. Veerabhadrappa Bidari, P. B. Nagaraj, and G. Lalagi, "Influence of different types of vortex generators (VGs) to enhance heat transfer performance in heat exchangers: a review," *International Journal of Ambient Energy*, pp. 1–24, 2021.

[42] H. Z. Han, B. X. Li, H. Wu, and W. Shao, "Multi-objective shape optimization of double pipe heat exchanger with inner corrugated tube using RSM method," *International Journal of Thermal Sciences*, vol. 90, pp. 173–186, 2015.

[43] P. K. Swamee, N. Aggarwal, and V. Aggarwal, "Optimum design of double pipe heat exchanger," *International Journal of Heat and Mass Transfer*, vol. 51, no. 9-10, pp. 2260–2266, 2008.

[44] Z. Iqbal, K. S. Syed, and M. Ishaq, "Optimal fin shape in finned double pipe with fully developed laminar flow," *Applied Thermal Engineering*, vol. 51, no. 1-2, pp. 1202–1223, 2013.

[45] Z. Iqbal, K. S. Syed, and M. Ishaq, "Optimal convective heat transfer in double pipe with parabolic fins," *International Journal of Heat and Mass Transfer*, vol. 54, no. 25-26, pp. 5415–5426, 2011.

[46] C. K. Kwong and H. Bai, "A fuzzy AHP approach to the determination of importance weights of customer requirements in quality function deployment," *Journal of intelligent manufacturing*, vol. 13, no. 5, pp. 367–377, 2002.

[47] S. Yijie and S. Gongzhang, "Improved NSGA-II multi-objective genetic algorithm based on hybridization-encouraged mechanism," *Chinese Journal of Aeronautics*, vol. 21, no. 6, pp. 540–549, 2008.

[48] T. A. Khan and W. Li, "Optimal design of plate-fin heat exchanger by combining multi-objective algorithms," *International Journal of Heat and Mass Transfer*, vol. 108, pp. 1560–1572, 2017.

[49] J. Zheng, R. Shen, and J. Zou, "Enhancing diversity for NSGA-II in evolutionary multi-objective optimization," in *Proceedings of the 2012 Eighth International Conference on Natural Computation (ICNC)*, pp. 654–657, IEEE, Sichuan, China, 2012, May.

[50] S. Chamoli, "Preference selection index approach for optimization of V down perforated baffled roughened rectangular channel," *Energy*, vol. 93, pp. 1418–1425, 2015.

[51] C. S. Dhanalakshmi, M. Mathew, and P. Madhu, "Biomass material selection for sustainable environment by the application of multi-objective optimization on the basis of ratio analysis (MOORA)," in *Materials, Design, and Manufacturing for Sustainable Environment*, pp. 345–354, Springer, Singapore, 2021.

[52] M. Mmohammadiun, F. Dashtestani, and M. Alizadeh, "Exergy prediction model of a double pipe heat exchanger using metal oxide nanofluids and twisted tape based on the artificial neural network approach and experimental results," *Journal of Heat Transfer*, vol. 138, no. 1, Article ID 011801, 2016.

[53] W. Liu, P. Liu, J. B. Wang, N. B. Zheng, and Z. C. Liu, "Exergy destruction minimization: a principle to convective heat transfer enhancement," *International Journal of Heat and Mass Transfer*, vol. 122, pp. 11–21, 2018.

[54] D. R. Fernandes, C. Rocha, D. Aloise, G. M. Ribeiro, E. M. Santos, and A. Silva, "A simple and effective genetic algorithm for the two-stage capacitated facility location problem," *Computers & Industrial Engineering*, vol. 75, pp. 200–208, 2014.

[55] T. L. Saaty and H. T. M. A. Decision, "How to make a decision: the analytic hierarchy process," *European Journal of Operational Research*, vol. 48, no. 1, pp. 9–26, 1990.

[56] A. V. L. N. Sujith, R. Swathi, R. Venkatasubramanian et al., "Integrating nanomaterial and high-performance fuzzy-based machine learning approach for green energy conversion," *Journal of Nanomaterials*, vol. 2022, Article ID 5793978, 11 pages, 2022.

[57] P. J. M. Van Laarhoven and W. Pedrycz, "A fuzzy extension of Saaty's priority theory," *Fuzzy Sets and Systems*, vol. 11, no. 1-3, pp. 229–241, 1983.

[58] C. S. Dhanalakshmi, P. Madhu, A. Karthick, M. Mathew, and R. Vignesh Kumar, "A comprehensive MCDM-based approach using TOPSIS and EDAS as an auxiliary tool for pyrolysis material selection and its application," *Biomass conversion and biorefinery*, pp. 1–16, 2020.

[59] P. Madhu, C. Nithiyesh Kumar, L. Anojkumar, and M. Matheswaran, "Selection of biomass materials for bio-oil yield: a hybrid multi-criteria decision making approach," *Clean Technologies and Environmental Policy*, vol. 20, no. 6, pp. 1377–1384, 2018.

[60] P. Madhu, C. Sowmya Dhanalakshmi, and M. Mathew, "Multi-criteria decision-making in the selection of a suitable biomass material for maximum bio-oil yield during pyrolysis," *Fuel*, vol. 277, Article ID 118109, 2020.

[61] M. Ilangkumaran, V. Sasirekha, L. Anojkumar et al., "Optimization of wastewater treatment technology selection using hybrid MCDM," *Management of Environmental Quality: An International Journal*, vol. 24, no. 5, pp. 619–641, 2013.

[62] M. Ilangkumaran and S. Kumanan, "Application of hybrid VIKOR model in selection of maintenance strategy," *International Journal of Information Systems and Supply Chain Management*, vol. 5, no. 2, pp. 59–81, 2012.

[63] M. Yazdani and A. F. Payam, "A comparative study on material selection of microelectromechanical systems electrostatic actuators using Ashby, VIKOR and TOPSIS," *Materials and Design*, vol. 65, pp. 328–334, 2015.

[64] L. Anojkumar, M. Ilangkumaran, and M. Vignesh, "A decision making methodology for material selection in sugar industry using hybrid MCDM techniques," *International Journal of Materials and Product Technology*, vol. 51, no. 2, p. 102, 2015.

[65] C. Thianpong, P. Eiamsa-ard, P. Promvonge, and S. Eiamsa-ard, "Effect of perforated twisted-tapes with parallel wings on heat tansfer enhancement in a heat exchanger tube," *Energy Procedia*, vol. 14, pp. 1117–1123, 2012.

[66] T. Murata and H. Ishibuchi, "MOGA: multi-objective genetic algorithms," *Evolutionary Computation IEEE International Conference on*, vol. 1, p. 289, 1995.